CHALMERS
UNIVERSITY OF TECHNOLOGY

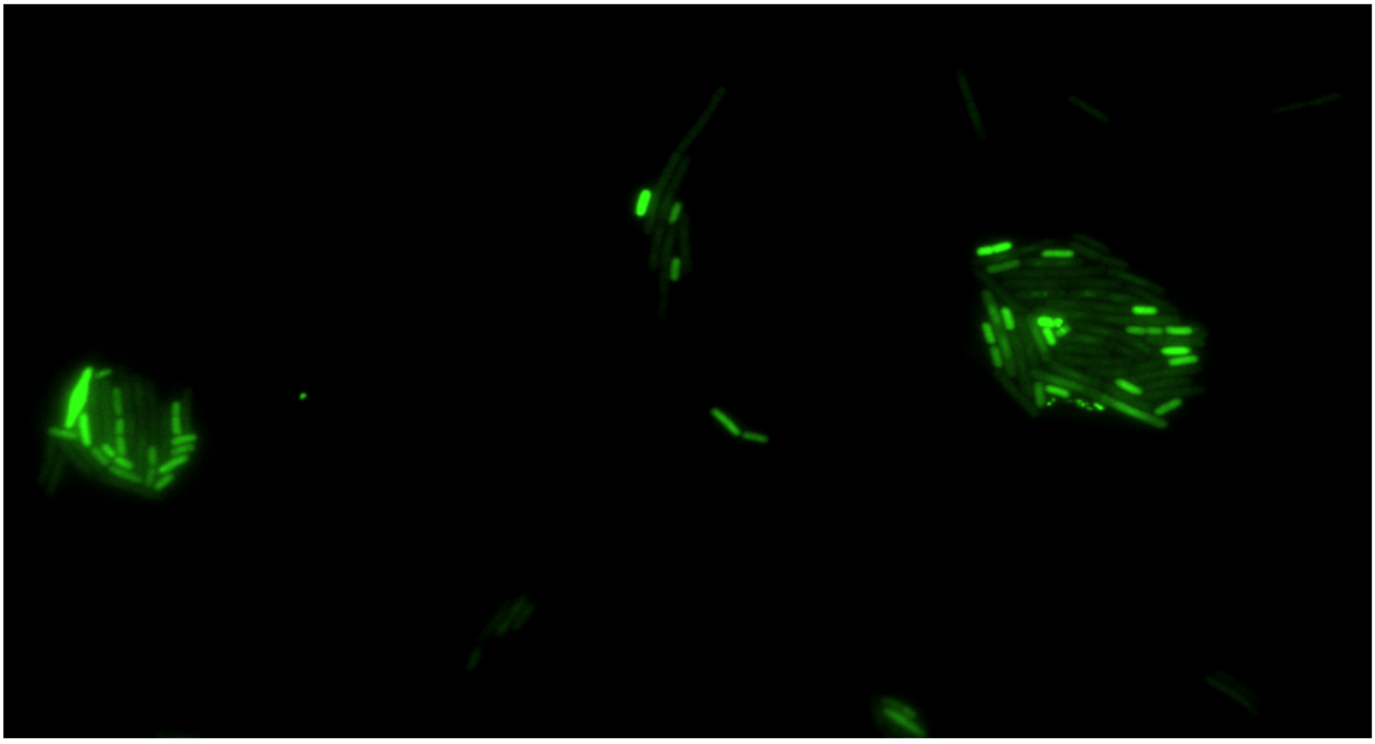

Master's thesis in

# UNCOVERING THE MECHANISM OF ACTION OF A NOVEL RUTHENIUM-BASED ANTIBIOTIC

## A multi-assay approach


BY: ROBIN RYDBERGH
EXAMINER: MICHAELA WENZEL
SUPERVISOR: ANN-BRITT SCHÄFER

**DEPARTMENT OF LIFE SCIENCES**
CHALMERS UNIVERSITY OF TECHNOLOGY



Gothenburg, Sweden 2025

# Abstract

Historically, metal containing compounds (MCC) have demonstrated significant therapeutic potential both as antimicrobial agents and for cancer treatment. MCCs represent some of the oldest antimicrobial compounds known such as *Salvarsan*, the first antibiotic discovered. This study investigates a novel ruthenium-based complex (Ru) for its antibacterial properties. Thorough knowledge of the mode of action (MoA) is a crucial step in the development of new antimicrobial compounds. In this study, a multi-assay investigative approach was employed to investigate the MoA of Ru in the Gram-positive model organism *Bacillus subtilis*. Initial inhibition activity experiments revealed that the Ru compound exhibits a minimum inhibitory concentration (MIC) of 6.25 μM.

In this study, bacterial cytological profiling showed indication of broad cellular disturbances. Most notably, a proteome-wide protein degradation effect was observed. Further, the membrane was disturbed, and DNA damage was detected. A novel assay measuring the induced protein degradation with different reactive oxygen species scavengers provided an unexpected and striking result. This provided evidence that oxidative stress, specifically caused by hydroxyl radicals rather than superoxide radicals, are a central part of the MoA. Additional microscopy with a superoxide radical probe further suggests that Ru appears to reduce the intracellular superoxide concentrations.

Collectively, these findings indicate a MoA where Ru causes oxidative stress which then leads to macromolecular damage and rapid protein degradation. The new scavenger assay results were particularly interesting and brought compelling insights, in which the presence of a hydroxyl radical scavenger stopped the rapid protein degradation induced by Ru. Understanding this novel MCC, which exhibits this unique rapid protein degradation MoA, could significantly advance the understanding towards innovation of new antibiotics in the important fight against antibiotic resistance.

# Acknowledgements

I would like to sincerely thank Ann-Britt Schäfer for her exceptional guidance, valuable insights, and dedication in supervising this project, I have learnt a lot. I am also grateful to Michaela Wenzel, both as an examiner and for providing thorough and constructive feedback which was very useful for the shaping of my thesis. Additionally, I appreciate the helpful guidance of Jonatan Nordborg and Margareth Sidarta with instrumentation and consultation on certain practical aspects of my experiments. The collaborative atmosphere within the group has been enjoyable and helped my development and the successful completion of this work.

# Disclaimers

During the writing process the generative text models ChatGPT o3 and 4.5 (OpenAI, United States) have been used in a responsible capacity for certain parts of the text. To accelerate writing I first provided crude drafts of content which I restructured using ChatGPT. This new structured draft I then heavily modified and thoroughly reviewed for language and factual accuracy towards a final state of the text. To accelerate parts of image analysis, software specific scripting was additionally programmed through iterative guided use of ChatGPT in which I do not take credit or claim for the code generated.

# Abbreviations

| | |
|---|---|
| AB | Antibiotic |
| AMR | Antimicrobial resistance |
| BCP | Bacterial cytological profiling |
| *B. subtilis* | *Bacillus subtilis* |
| CMR | Carcinogenic, mutagenic and reprotoxic chemical |
| DAPI | 4′,6-diamidino-2-phenylindole |
| DMSO | Dimethyl sulfoxide |
| DNA | Deoxyribonucleic acid |
| GFP | Green-fluorescent protein |
| GMO | Genetically modified organism |
| $H_2O_2$ | Hydrogen peroxide |
| LB | Lysogeny broth |
| MeA | Mechanism of action |
| MoA | Mode of action |
| MitC | Mitomycin C |
| MIC | Minimal inhibitory concentration |
| MCC | Metal-containing compounds |
| Nis | Nisin |
| NR | Nile red (9-diethylamino-5H-benzo[α]phenoxazine-5-one) |
| $O_2^{\bullet -}$ | Super oxide radical |
| OD | Optical density |
| OH• | Hydroxyl radical |
| OSC | Optimal stressor concentration |
| PBS | Phosphate-buffered saline |
| PET-G | Polyethylene terephthalate glycol |
| ROS | Reactive oxygen species |
| RNS | Reactive nitrogen species |
| RNA | Ribonucleic acid |
| RPM | Revolutions per minute |

# Table of Contents

# 1. Introduction

## 1.1 Early use of metals in medicine

Historically, metal-containing compounds (MCC) have attracted interest due to their medicinal applications. One prominent early example is arsphenamine (*Salvarsan*), an arsenic-based compound identified by Paul Ehrlich in 1910. *Salvarsan* is recognized as the first effective modern antibiotic, particularly revolutionary to treat syphilis that had no treatments known at the time [1].

Later MCCs have most notably been used in cancer treatment, where research led to the development of cisplatin in the 1960s. This platinum-based chemotherapy agent exhibits an antitumor effect primarily by formation of DNA adducts and induction of apoptosis [2]. MCCs have also been explored for their therapeutic properties with relation to Malaria. For example, the organometallic agent ferroquine, has shown promising potency against chloroquine-resistant *Plasmodium* strains [3].

Over time, research into MCC activity and toxicity profiles has encouraged a shift towards further investigation of these compounds as candidates for new antibiotics. In present times, research on MCCs is a growing field in efforts to discover novel antimicrobial agents as MCCs have unique chemical properties compared to conventional small molecule antibiotics [4]. Notably, in screenings conducted by the Community for Open Antimicrobial Drug Discovery (CO-ADD), MCCs exhibited a remarkably high antibacterial hit rate of 27%, compared to only 1.6% for purely organic molecules, highlighting their potential for antibiotic research. Close to 10% of the MCCs identified as active were non-toxic to human cells, greatly exceeding the general hit rate observed in conventional compound libraries [5]. MCCs have been shown to have activity for both Gram-positive (G(+)) and Gram-negative (G(-)) bacteria and even against MRSA (methicillin-resistant *Staphylococcus aureus*) bacteria. Despite toxicity concerns, MCCs hold promise for expanding the antibiotic arsenal, which is of the outmost importance at the present in the race against antimicrobial resistance [6][7][8].

## 1.2 Choice of model organism

This study utilizes the bacterium *Bacillus subtilis* (*B. subtilis*) to elucidate the effects of antibiotic compounds on bacterial cells. This model organism is widely recognized for studying Gram-positive (G(+)) bacteria [9]. It is non-pathogenic, easy to work with, and has the Generally Regarded As Safe (GRAS) status [10]. It is the most well-studied Gram-positive model organism in bacterial cell biology. It has extensive and developed proteomic as well as genomic databases with genetic manipulation tools [9] [11]. *B. subtilis* has also been extensively used as a model organism to study antibacterial modes of action (MoA) at the cellular level with a wide range of analytical tools developed. Because *B. subtilis* is closely related to important pathogens, the findings derived from studies using *B. subtilis* generally translate effectively to pathogenic bacteria. Being non-pathogenic itself while still a valid model for pathogen analogues makes it a great choice for antibiotics research [12][13].

## 1.3 Previous investigation of the Ruthenium compound's MoA

Through research collaboration between the *Frei Lab* (University of York, England), and the *Wenzel Lab* (Chalmers University of Technology, Sweden), a set of metal-based antibiotic compounds with preliminary confirmed therapeutic effects was assigned for investigation. One of these compounds, a ruthenium-based complex (Ru), had measured activity against Gram-positive bacteria and was examined using a series of assays to begin investigating its MoA.

To start the journey of investigation, *B. subtilis* was chosen as the model organism and initial experiments were carried out. First, to determine the activity of the new antibiotic, the minimal inhibitory concentration (MIC) and the optimal stressor concentration (OSC) was determined (*A.B. Schäfer and C. Özsan, unpublished*). Then, green fluorescent protein (GFP) dependent localization assays for the MreB and MinD proteins were attempted, however the experiments consistently failed due to disruptions observed in the GFP signal.

To follow up this decrease in GFP, a *PrpsD-gfp* (*gfp*-gene with strong constitutive promotor) spectroscopy assay was performed to assess whether Ru affects translation or causes degradation of the GFP protein. Using known translation inhibitors (kanamycin and chloramphenicol) and a pore-forming antibiotic (nisin) as positive controls, the spectroscopy results (*Figure 1A*) showed that only the Ru caused a significant reduction in GFP signal. This suggests a potential protein degradation and excluding inhibition of protein synthesis or GFP leakage (*A.B. Schäfer* and *E. van Leuven, unpublished*). A Western blot was used for the red fluorescent protein mCherry (*Figure 1B*) that revealed a substantial loss of mCherry during Ru treatment (*G.Marinho Righetto, unpublished*). This further points at proteolysis and that the degradation is not specific to GFP. Non-protein fluorescent dyes remained unaffected and a subsequent spectral scan of mCherry and GFP with Ru was done which confirmed that there was no spectral interference causing the degradation (*A.B. Schäfer, unpublished*). Following this, an SDS-PAGE (*Figure 1C*) revealed a proteome-wide protein depletion after Ru treatment independently of fluorescent tags (*A.B. Schäfer and E. van Leuven, unpublished*).

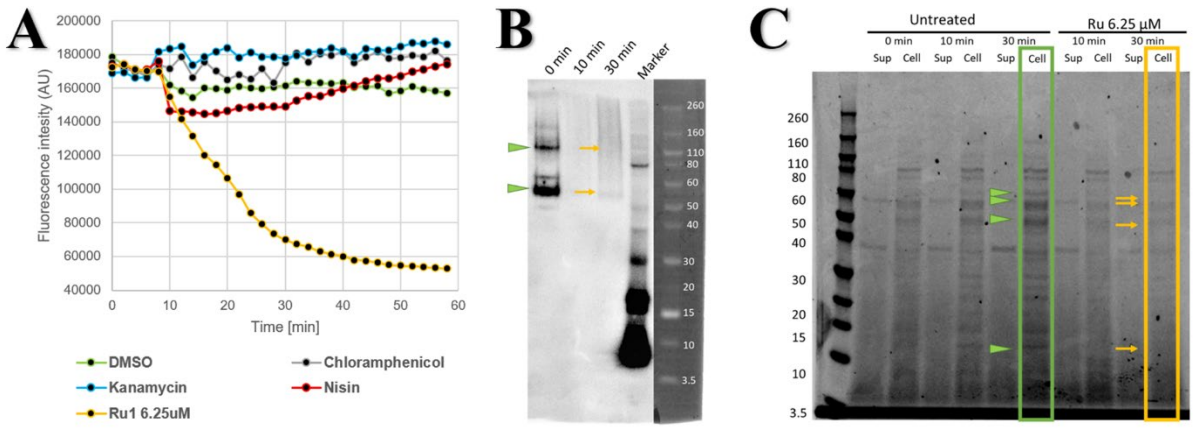


**Figure 1. Key results from previous studies: GFP Spectroscopy (A), mCherry Western blot (B), and SDS-PAGE (C).** In **A**, a clear decline in GFP intensity is visible for Ru-exposed samples, whereas GFP in the other samples remain relatively stable. In **B** and **C**, green arrows indicate dominant protein bands, while yellow arrows highlight the expected positions of these proteins post Ru exposure. **B** shows marked disappearance of mCherry bands at 10- and 30-min. **C** illustrates overall protein depletion in Ru-exposed cells at these same intervals, while supernatant protein content remains largely unchanged.

Taken together, these initial results lead to the hypothesis that Ru appears to cause a non-selective protein degradation, either mediated by multiple proteases or in an entirely protease-independent manner. Single deletion mutants devoid of certain intracellular proteases then revealed that the Ru-induced protein degradation did not seem to be mediated by intracellular proteases (*R. Rani, unpublished*). Finally, a MIC assay with addition of reactive oxygen species (ROS) scavengers significantly reduced the activity of Ru (*R. Rani, unpublished*), which indicated that a protease-independent mechanism could possibly be related to oxidative damage. Additional assays to rule out direct effects on the membrane were also carried out. A propidium iodide assay showed no increase in membrane permeability and a DisC35 assay, designed to measure membrane depolarization revealed no significant loss of potential (*A.B. Schäfer and C. Özsan, unpublished*). These results rule out Ru antimicrobial activity is caused directly by affecting the membrane.

## 1.4 Hypotheses

From these previous studies, the following hypotheses were deduced:

- **Hypothesis 1: Impaired protease target acquisition**
  Ru alters active proteases to become indiscriminate in their protein recognition/degradation.
- **Hypothesis 2: Protease disruption**
  Ru activates promoters causing upregulation of one or more bacterial proteases, which may lead to a shift in the protein turnover.
- **Hypothesis 3: Protein misfolding**
  Ru causes proteins to misfold, which make them susceptible to degradation by cytosolic proteases.
- **Hypothesis 4: Oxidative stress-related protein degradation**
  Ru induces substantial oxidative stress that damage DNA, proteins, and membranes.

## 1.5 Aims

This master's thesis aims to contribute to the work of elucidating the mode of action by which the ruthenium complex induces protein degradation. The approach involves examining the bacterial cytology and oxidative stress systems to provide further insights.

### Limitations

This project will assess general trends with connection to proteolytic activity with focus on oxidative stress rather than examining individual proteases in detail as this had previously shown little connection. Due to practical constraints such as time and resources, orthogonal assays for validation will not be carried out and assay optimization will be limited to making reproducible results. Within the scope of this thesis, new hypotheses emerging from experiment analysis will not be experimentally pursued. Comprehensive mechanistic validation of the precise targets or interactions will be the focus of future studies.

## 1.6 Importance and ethical considerations

Antibiotic resistance has become a global threat with high levels of resistance in some regions of the world. There is an urgent need to develop new antibiotics that can effectively combat emerging diseases and pathogens.

This work aims to contribute to that effort by exploring a novel metal complex-based antibiotic with a unique mode of action, potentially opening a new branch of therapeutic strategies. By advancing our understanding of this unique compound and its mechanism of action, we can actively contribute to the fight against antimicrobial resistance.

This study uses bacteria as a model organism and does not harm sentient organisms or animals. While the chosen bacterium has GRAS status, the strains used in this study are genetically modified and carry antibiotic resistance genes, which could, if not properly contained and worked with, spread outside the lab and decrease the effectiveness of life-saving antibiotics. This risk is mitigated by following the proper laboratory routines. For this study, the importance and promise of insights into new antibiotics is considered to outweigh the risks.

## 2. Theoretical Background

In this study, antibiotics and their effects have been evaluated in bacteria using multiple fluorescence-based measurement techniques. The theoretical background will provide more detailed information about techniques and biological processes which are relevant to the project such as for reactive oxygen species and proteases.

### 2.1 The model organism

#### 2.1.1 Gram-positive and Gram-negative bacteria

Bacteria can be classified into two groups: G(+) or G(-). They differ in the composition of their cell envelopes. While G(+) species have a single membrane surrounded by a thick peptidoglycan layer, G(-) bacteria possess an additional outer membrane surrounding a thinner layer of peptidoglycan. This difference in cell envelope structure influences bacterial susceptibility to antibiotics, while inherent biological effects within the cytosol are similar among different types of bacteria [9][14][15]. New antibiotics are typically screened for potency in both G(+) and G(-) bacteria to test if they display antibiotic properties in either. For this study, Ru was found to have an antibiotic effect on G(+) bacteria.

Although G(+) and G(-) bacteria differ most notably in their cell envelope structures, their core molecular machinery (DNA replication, transcription and translation) is similar. Studies in non-pathogenic G(+) models such as *B. subtilis* can therefore provide useful insight into fundamental antibiotic mechanisms that may be adapted for targeting G(+) pathogens (*M. Sidarta and Shubda. Dev, personal communication*, February 14, 2025).

#### 2.1.2 *Bacillus subtilis*

*B. subtilis* is a G(+), aerobic, spore-forming bacterium in the shape of straight rods. Depending on growth stage these rods measure between 2–6 µm long and around 0.7 µm diameter [16]. After cellular division, daughter cells often remain attached, which causes *B. subtilis* to grow in long multicellular chains [17]. Under nutrient-abundant conditions at 37 °C, the doubling time is around 20 min. Less hospitable conditions can be used to mimic different stress conditions and cause slower growth and doubling times of 40 min and longer [16] [18].

#### 2.1.3 Proteases and their role in *B. subtilis*

For Ru, an initial finding was a rapid degradation of proteins, leading to *hypothesis 1-3,* which suggests that proteases could be involved in the MoA. Proteases are catalytic enzymes that are essential for protein catabolism and thus homeostasis, making them central to cellular function in *B. subtilis* [19]. Proteases have different functions and are divided into function-depending classes such as the serine, cysteine, aspartic, and metallo-proteases. Different protease classes are involved in different activities like protein folding quality control, regulatory proteolysis, and nutrient scavenging [20]. Protease activity is generally regulated by stress responses and growth phase-related signals, i.e. stress factors can increase expression of certain proteases while starvation induces another set of proteases [20]. Protease dysregulation, as seen with acyldepsipeptides, can lead to uncontrolled protein degradation by de-regulation of ClpP, highlighting proteases as potential targets for antibiotic development [21].

### 2.1.4 Reactive oxygen species in *B. subtilis*

Another factor that can play a role in the mode of action of a compound are ROS. ROS have a natural cytosolic presence in bacteria and are formed to a certain degree during bacterial metabolism. This ROS are primarily caused by release of electrons from the aerobic electron transport chain, in which molecular oxygen unintentionally captures electrons generating superoxide radicals (O2•–) (*see figure 2*) [22][23]. These superoxide radicals are highly reactive and can damage essential macromolecular components like the DNA, proteins, and lipids [24]. To manage the superoxides, bacteria utilize a family of enzymes called superoxide dismutases (SOD). These enzymes have metal catalytic sites, usually iron or manganese, that can convert O2•– into the less reactive hydrogen peroxide ($H_2O_2$) [24]. $H_2O_2$ is still a moderately reactive oxygen species that can be converted to highly aggressive hydroxyl radicals (•OH) by the Fenton reaction. Therefore, $H_2O_2$ is further reduced by bacterial enzymes such as catalases and peroxidases, which both can convert $H_2O_2$ to water [24]. Additional ROS specialized antioxidant compounds called scavengers can reduce ROS to water in redox reactions which further protect from intracellular oxidative stress. In *B. subtilis* there is a scavenger called bacillithiol which can be regenerated similar to the glutathione scavenger in other organisms [25][26].

If hydroxyl radicals are formed, [27], they can rapidly damage critical macromolecules such as the DNA, proteins, and membrane lipids [27][25]. Bacteria have a diminished ability to detoxify hydroxyl radicals, making them more susceptible to oxidative damage caused by •OH [27]. Bacteria are also generally less efficient than eukaryotic cells in managing ROS. This is something that our bodies through the immune system exploit as a measure of defence to kill bacteria.

This described inherent lower ability in bacteria to handle ROS also makes it a promising target for antibiotic development [25]. To selectively investigate ROS in bacteria, one can employ mutants deficient in either SOD or catalase/peroxidase enzymes. Alternatively, application of specific scavengers such as tiron for superoxide and thiourea for hydroxyl radicals or fluorescent probes such as Oxyburst [28] [29][30][31].

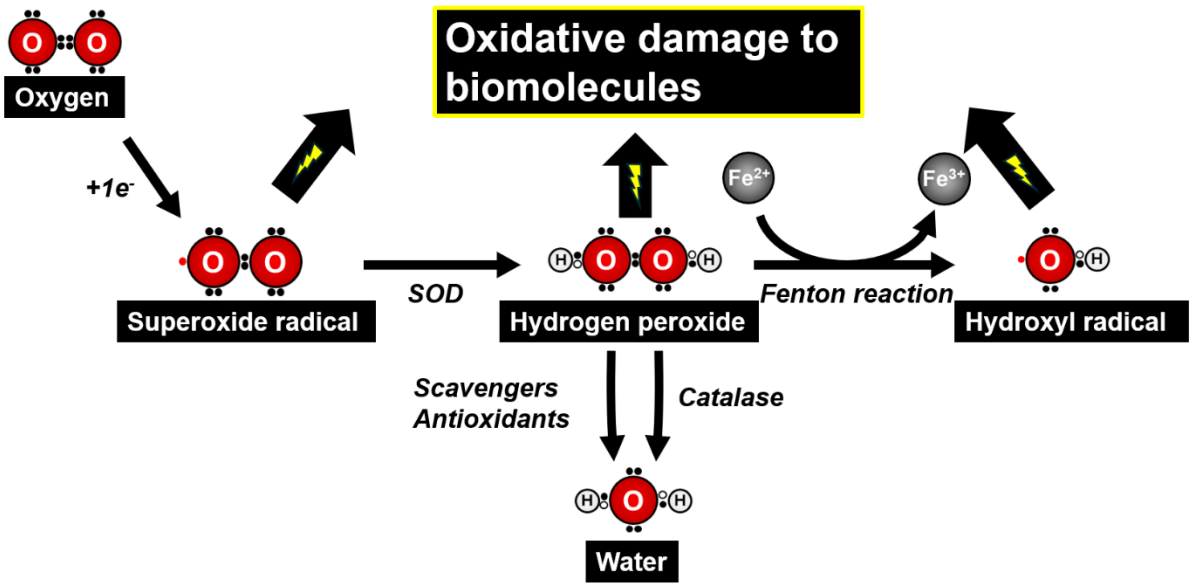


**Figure 2, Overview of bacterial ROS reactions.** Arrows represent conversions between different forms of oxygen species, in which oxygen atoms are red and hydrogen light grey. Black dots represent electrons, hollow dots represent hydrogen electrons and red dots represent a radical unpaired electron. SOD: Superoxide dismutase; GSH: glutathione; GR: glutathione reductase, GPx: glutathione peroxidase.

## 2.2 The use of fluorescence

Many reporters utilized to obtain information in biological systems are based on the use of fluorescent compounds and proteins. These reporters can be studied in cells using microscopes specifically adapted to image fluorescence.

### 2.2.1 Fundamentals of fluorescence

Fluorescence is a type of light emission, in which a substance absorbs light at one wavelength and then quickly emits light of lower energy at a longer wavelength [32]. When a molecule absorbs light, one of its electrons is excited to a higher energy state (*see Figure 3B*). While in the excited state, the electron loses energy through, e.g., vibrations in a process known as non-radiative transitions, causing the electron to drop to a lower energy level within the excited state. When the electron returns to the ground state, it releases a photon in the process. This emitted photon has lower energy and thus has a longer wavelength than the absorbed light. The difference in wavelength between the absorbed and emitted light is what is known as the Stokes shift (*see Figure 3D*).

Molecules with fluorophores have the unique property to emit fluorescent light at a longer wavelength determined by the Stokes shift. Some molecules in biology are naturally fluorescent, such as tryptophan (Trp), phenylalanine (Phe), and tyrosine (Tyr), while others are synthetically designed to be fluorescent like dyes that are introduced into otherwise non-fluorescent systems [32]. A naturally occurring fluorescent protein with a fluorophore is the green-fluorescent protein (GFP). GFP has a barrel structure with a central fluorophore composed of three amino acids [33]. The fluorophore can absorb light and, through the same process described above, emit fluorescent light (*see Figure 3 A and C*). GFP can be introduced into non-fluorescent systems to enable the study of gene expression and protein behavior in cells and whole organisms [34]. In this study, GFP along with the fluorescent dyes Nile Red, Oxyburst, and DAPI are used for cytological profiling of *B. subtilis*.

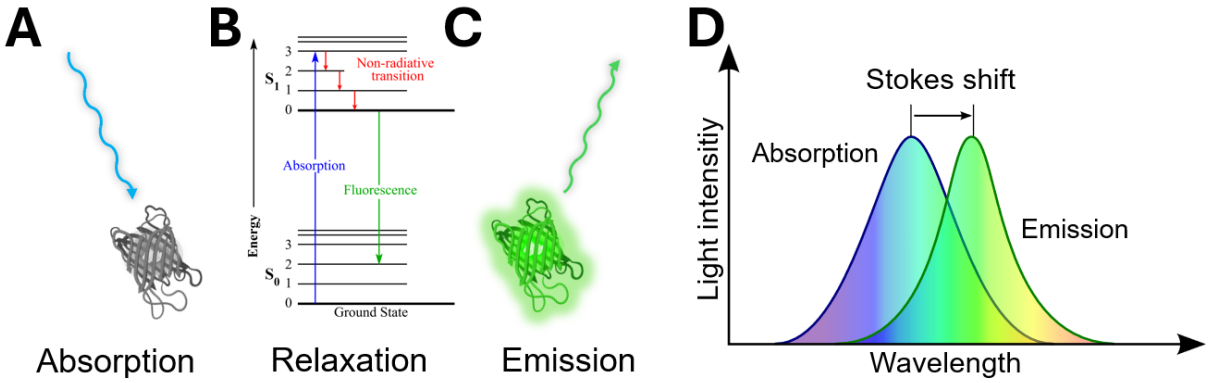


**Figure 3, concepts of fluorescence.** A GFP absorbing a photon (A), the fluorescent process of excitation-relaxation and emission in a Jablonski diagram (B), a GFP emitting a photon (C), and a diagram that shows the concept of the Stokes shift (D) [35][36].

### 2.2.2 Fluorescence dependent approaches to study effects of antibiotics

For an antibiotic to be used it is important that its antibiotic activity is understood. MoA studies employed to this end consist of a multitude of assays to investigate biological changes due to antibiotic treatment throughout the cell. Bacterial cytological profiling (BCP) is a popular fluorescence microscopy method for rapid MoA analysis as it gives an overview of different cellular components. In this approach, bacteria are imaged after a short exposure to an antibiotic followed by staining with both membrane- and DNA-specific fluorophores. Through image analysis, the resulting morphological descriptors such as the cell length and width, nucleoid organization, membrane integrity, and permeability can be analyzed with principal component analysis to generate a "cytological fingerprint". This idea originated in a study by Pogliano and co-workers that showed how fingerprints obtained from BCP could cluster 30 reference antibiotics into their correct mechanistic classes with high accuracy [37]. This screening can be expanded by for example introducing state sensitive lipid phase probes or GFP-tagged reporter proteins that further enable the method to resolve specific cellular effects and reveal effects on multiple cellular targets [38][39].

A range of GFP-tagged proteins are also available, these can give useful insights about the stress state of bacteria. An example of this is the RecA protein, which acts as frontline DNA-repair protein in *B. subtilis.* When the bacterial chromosomal DNA is damaged or a replication fork stalls, the loader proteins RecO and RecR place the RecA protein onto exposed single-stranded DNA [40]. The recruitment of RecA and subsequent indication of DNA damage can be visualized by fusing this protein to a fluorescent tag. In this study, BCP was used to obtain an overview of cellular stress and a RecA-GFP fusion was utilized to investigate DNA damage caused by Ru.

# 3. Methodology

Here the methodology for the conducted assays MIC, acute stress, BCP, RecA-GFP, Oxyburst microscopy, and GFP scavenger spectroscopy are presented in further detail. Detailed information on all reagents, materials, and instruments used within this study can be found in *3.1.6 Reagent and consumable inventory*.

## 3.1 General laboratory procedures

### 3.1.1 Growth conditions

All sterile work was carried out using a gas flame to produce a work area of continuous up-draft. Unless stated otherwise, *B. subtilis* cultures were grown under constant agitation at 37 °C in a water-bath. Inoculations and dilutions were performed with a working volume of 2 mL in 50 mL conical "*Falcon*" polypropylene tubes. Overnight cultures were prepared by inoculation from a glycerol stock and grown overnight for a maximum of 16 h. Overnight cultures were then diluted into fresh medium on the day of experimentation.

Filter sterilization of media and stock solutions used 0.22 µm Millex-GP syringe filter units. Cell density ($OD_{500}$ for PBS solutions and $OD_{600}$ for LB) was consistently measured on a GENESYS 30 visible spectrophotometer using a 1 : 10 culture-to-medium dilution in plastic cuvettes, each mixed by aspiration to ensure homogeneity before measurement. All water preparations were made with ultrapure Milli-Q (mQ) water.

### 3.1.2 Media preparation

Lysogeny broth (LB) was prepared by dissolving 10 g NaCl, 10 g tryptone, and 5 g yeast extract per liter. The media was adjusted to a pH of 7.0 with 1 M NaOH/HCl. Media was autoclaved (121 °C, 20 min) to ensure sterility. Sugar solutions of glucose and xylose were prepared to 40% and 20% (w/v) of the respective sugars followed by filtration through Millex-GP units.

### 3.1.3 Antibiotic and dye handling

5 mM primary stocks of Ru were sterilely prepared in dimethyl sulfoxide (DMSO). Additionally, a nisin stock with 250 µg/mL and a mitomycin C (MitC) stock of 0.5 mg/mL were prepared sterilely in mQ. All the prepared antibiotic stock solutions were then aliquoted and stored at −20 °C. For each experiment, antibiotic aliquots were thawed and for Ru, working concentrations (625, 312.5, 156.25 µM) were freshly prepared in DMSO before each experiment and discarded after use.

Fluorescent dyes were thawed for at least one hour before use, vortexed to ensure homogeneity and, in the case of Nile red (NR), centrifuged for 30 s in a bench-top microfuge. The dye stocks for DAPI dihydrochloride, OxyBURST™ Green $H_2$DCFDA succinimidyl ester (Oxyburst), and Nile red are light sensitive and were handled in non-translucent, black containers.

### 3.1.4 Strains and glycerol stocks

Strains of *B. subtilis* grew in LB medium with added different supplements for some strains listed in *Table 1*. Cultures of UG10 received spectinomycin (100 µg/mL) and were additionally supplied with 0.5% (w/v) xylose to induce the RecA-GFP fusion protein. When cultures reached $OD_{600} \approx 1600$ µL of cell suspensions were mixed separately with 400 µL of sterile 50% glycerol each, yielding 20% (v/v) final glycerol concentrations. The mixtures were vortexed briefly, dispensed into 1 mL cryovials, and stored at −80 °C for use in inoculations.

**Table 1, Strains of *B. subtilis* used in Ru assays.**

| Strain | Genotype / Modification | Source | Inducer | Reference |
|---|---|---|---|---|
| 168CA | *B. subtilis trpC2* (wild type) | DSMZ, Braunschweig, Germany | -- | [41] |
| UG-10 | *amyE::Pxyl-recA-mgfp* spc | derivative of 168CA (Wenzel Lab) | 0.5% Xylose | [42] |
| MW54 (bSS82) | *amyE::spc PrpsD-gfp* | derivative of 168CA (Wenzel Lab) | -- | [43] |

### 3.1.5 Safety considerations

All in-house confidential antibiotics of Ru along with MitC, were handled following procedures consistent with carcinogenic, mutagenic, and reproductive toxicity (CMR) guidelines. Genetically modified organism (GMO) strains employed in this project were handled with care and strict waste disposal protocols with waste autoclavation to mitigate potential release of mutations and antibiotic resistance was followed. Concentrated chemical solutions such as 0.5 M sodium hydroxide, 1 M hydrochloric acid, and 30% hydrogen peroxide were handled with care using appropriate personal protective equipment. Surface sterilization within the workspace was routinely performed using 70% ethanol and special caution was exercised when operating gas Bunsen burners near ethanol-disinfected surfaces to maintain sterility without fire hazards. Laboratory coats and safety glasses were always worn and laundered every three months or sooner if visibly dirty. Hazardous powders such as thiourea powder were weighed by shuttling a sealed 50 mL Falcon tube between a scale and a fume hood to eliminate aerosol formation. Waste disposal was conducted according to institutional hazardous waste guidelines. Here, chemical waste, GMO-contaminated materials, and sharp items were appropriately separated, labeled, and disposed of via specialized waste handling to ensure compliance with environmental and safety regulations.

### 3.1.6 Reagent and consumable inventory

Media components and general reagents are specified in *Table 2*, Antibiotics and fluorescent dyes in *Table 3*, and information about the instruments and consumables used in this project in *Table 4*.

**Table 2.** Media components and general reagents

| Reagent | Specification / grade | Catalogue no. | Supplier / Manufacturer |
|---|---|---|---|
| Glycerol | Molecular-biology grade | 10021083 | Fisher BioReagents |
| Trizma® HCl solution (1 M, pH 8.0) | Buffer | T2663 | Sigma-Aldrich |
| Dopamine HCl | ≥ 98% | 21992 | Cayman Chemical |
| Hydrochloric acid, 1 M | Analytical grade | – | Merck KGaA |
| Sodium hydroxide, 1 M | Analytical grade | – | Merck KGaA |
| Milli-Q water (18.2 MΩ cm) | Ultrapure | – | Sartorius |
| Agarose SPI | Molecular-biology grade | A1203.0100 | Duchefa Biochemie |
| Tryptone | Microbiological grade | 12787099 | Fisher Chemical |
| Yeast extract | – | Y1333.1000 | Duchefa Biochemie |
| Sodium chloride | Analytical grade | BP358212 | Fisher BioReagents |
| Glucose | Molecular-biology grade | – | Sigma-Aldrich |
| Xylose | ≥ 98% | X8008.0500 | Duchefa Biochemie |
| Dimethylsulfoxide | Anhydrous | D1370.0250 | Saveen & Werner / Duchefa |

**Table 3.** Antibiotics and fluorescent probes

| Compound | Function | Catalogue no. | Supplier / Manufacturer |
|---|---|---|---|
| Ru (novel ruthenium complex) | Antibiotic candidate | N/A | Frei Lab, Univ. of York |
| Nisin | Antibiotic | 155839 | Fisher Scientific / MP Biomedicals |
| Mitomycin C | Antibiotic | BP25312 | Fisher Scientific |
| Spectinomycin | Antibiotic | S0188.0025 | Saveen & Werner / Duchefa |
| Nile red | Membrane dye | N1142 | Fisher Scientific / Invitrogen |
| DAPI dihydrochloride | DNA dye | D1306 | Fisher Scientific |
| Oxyburst Green H2DCFDA, SE | ROS probe | D2935 | Fisher Scientific |

**Table 4.** Instrumentation and consumables

| Function | Item / specification | Catalogue no. | Manufacturer (city, country) |
|---|---|---|---|
| Syringe filter (sterile) | Millex GP PES 0.22 µm, 33 mm | SLGPR33RS | Merck Millipore, Carrigtwohill, Ireland |
| 96-well assay plate | Costar®, black/clear, flat-bottom | 3631 | Corning Inc., Kennebunk ME, USA |
| 96-well MIC plate | Falcon™ non-treated, flat-bottom | 353916 | Corning Inc., Kennebunk ME, USA |
| 50 mL conical tube | Falcon® polypropylene | 352070 | Corning Inc., USA |
| Plastic cuvette | PS, 10 mm path length (disposable) | 14-955-127 | Thermo Fisher Scientific, Waltham MA, USA |
| Plate reader | CLARIOstar Plus | 430-2544 | BMG Labtech, Ortenberg, Germany |
| Spectrophotometer | GENESYS 30 | 9A1A013133 | Thermo Fisher Scientific, Waltham MA, USA |
| Water-bath incubator | H 20 SOW | L002910 | Lauda Dr. R. Wobser GmbH, Lauda-Königshofen, Germany |
| Thermoshaker | ThermoMixer F2.0 | 5387000013 | Eppendorf SE, Hamburg, Germany |
| Microcentrifuge | 24-place, up to 21,300 ×g (e.g., 5425 R) | 5405000488 | Eppendorf SE, Hamburg, Germany |
| Ultrapure-water system | arium® pro | – | Sartorius, Göttingen, Germany |
| Fluorescence microscope | Nikon Eclipse Ti2 inverted; CFI Plan Apo DM λ 100×/1.45 NA objective; PRIME BSI camera; Sola SE II FISH 365 LED; Okolab chamber | – | Nikon, Japan / Photometrics, USA / Lumencor, USA / Okolab, Italy |
| Multi-spot microscope slide | Epredia™ 12 × 9 mm Wells | 12392136 | Epredia, Portsmouth NH, USA |
| Glass coverslip | 24 × 60 mm, No. 1.5 | 0111540 | VWR International, Radnor PA, USA |

## 3.2 Antimicrobial activity assays

A MIC assay and a bacterial growth curve were performed to determine the activity of the Ru compound and to establish its optimal stressor concentration (OSC). Observations of bacterial cell death from high antibiotic concentrations alone provides limited mechanistic insights for antibiotic research. The OSC, which is the concentration that inhibits growth by 50-70% in the exponential growth phase, was determined to be used for exposures the in subsequent mode of action assays. These assays also assessed whether the compound retained efficacy after prolonged storage.

### 3.2.1 Minimal inhibitory concentration (MIC)

A minimal inhibitory concentration assay was performed according to a protocol by the clinical and laboratory standard institute [44]. *B. subtilis* 168CA was grown to an $OD_{600}$ ≈1, diluted to 1 × 10^6 CFU/mL, and 100 µL of this suspension was mixed 1 : 1 with 100 µL of antibiotic dilution in each well for a final concentration of 5 × 10^5 CFU/mL. The MIC layout was designed to test concentration gradients starting at 100 µM Ru, 8 µg/mL nisin, and 8% DMSO, as illustrated in the plate layout *Figure 4*. Twofold serial dilutions of antibiotics were prepared in a 96-well plate (Falcon™ 96-Well, clear non-treated, Flat-Bottom Microplate) before adding bacterial cells. The plate was measured for bacterial growth and monitored for 16 hours by absorbance measurements at 600 nm using the *CLARIOstar Plus* plate reader. Detailed instrument settings are available in *Appendix C: MIC settings*.

| | 1 | 2 | 3 | 4 | 5 | 6 | 7 | 8 | 9 | 10 | 11 | 12 |
|---|---|---|---|---|---|---|---|---|---|---|---|---|
| A | SC | 0.195 | 0.391 | 0.781 | 1.563 | 3.125 | 6.25 | 12.5 | 25 | 50 | 100 | GC |
| B | SC | 0.016 | 0.031 | 0.063 | 0.125 | 0.25 | 0.5 | 1 | 2 | 4 | 8 | GC |
| C | SC | 0.016 | 0.031 | 0.063 | 0.125 | 0.25 | 0.5 | 1 | 2 | 4 | 8 | GC |
| D | SC | | | | | | | | | | | GC |
| E | SC | | | | | | | | | | | GC |
| F | SC | | | | | | | | | | | GC |
| G | SC | | | | | | | | | | | GC |
| H | SC | | | | | | | | | | | GC |

DMSO [%]
nisin [µg/mL]
Ru [µM]

**Figure 4, Minimal inhibitory concentration plate layout.** Rows are indexed alphabetically, columns are indexed numerically. Columns 1 and 12 (white) served as controls (SC: sterile control; GC: growth control). Columns 2–11 contained gradient concentrations of Ru (red) in row A, nisin (light blue) in row B, and DMSO (light grey) in row C. Dark, grey-marked wells were not utilized.

### 3.2.2 Growth curve

For the acute shock assay, an overnight culture of the 168CA strain was diluted into 20 mL in a 100 mL culturing flask. The culture OD was measured every 30 minutes until reaching an $OD_{600}$ of 0.30. Afterwards, the culture was divided into 2 mL aliquots and antibiotics were added to final concentrations of 1.5625, 3.125, and 6.25 µM Ru, 0.2, 0.4, 0.6, and 0.8 µg/mL nisin, and one untreated control. Post antibiotic addition, ODs were recorded every 15 minutes for four hours under semi-sterile conditions. Time points and corresponding OD measurements for each treatment were documented.

## 3.3 Fluorescence microscopy

Fluorescence microscopy was performed on a Nikon Eclipse Ti2 inverted microscope equipped with a CFI Plan Apochromat DM λ 100×/1.45 NA oil-immersion objective (working distance 0.13 mm), a PRIME BSI sCMOS camera (Photometrics, USA), a Sola SE II FISH-365 LED light source (Lumencor, USA), the NIS elements AR software version 5.42.02 software and an environmental control chamber (Okolab SRL, Italy) . The microscope is equipped with standardized filters optimal for GFP, RFP (used for NR imaging) and DAPI.

### 3.3.1 Agarose solution preparation and handling

To cast microscopy glass slides with thin agarose layers, a 1.2% agarose solution was prepared in advance according to method described in [45]. In short, 1.2% agarose solution was made and heated in a microwave until boiling in multiple cycles until all agarose was dissolved. The agarose solution was then stored in a 65 °C oven until use.

### 3.3.2 Polydopamine coating of coverslips

Coverslips (24 × 60 mm) were loaded into 3D-printed PET-G plastic racks (*designed in this project, see Appendix B*). In a first step they were rinsed with mQ water and then submerged in a freshly prepared 2 mg/mL dopamine hydrochloride solution containing 1 mM Tris-HCl, pH 8.0. Coverslips were treated for 30 min at room temperature while shaded from external light. After two rinses in mQ, the coverslips in the rack were dried at 37 °C for approximately 1-2 hours.

### 3.3.3 Sample preparation

15-30 minutes before microscope imaging, 700 µL of the prepared 65 °C 1.2% agarose solution was applied on top of a multi spot slide and a regular glass slide was used to press the agarose in a thin consistent layer. Before use, the top microscope glass slide is carefully removed exposing the cast agarose layer on the multi-spot slide ready to be used.

Three minutes before imaging, a freshly cast agarose-covered multi-spot slide was retrieved and 0.5 µL of bacterial culture of each sample was gently pipetted onto the solidified agarose. After excess culture medium had evaporated, the agarose slide was covered with a glass coverslip. A drop of immersion oil was applied, and the slide was transferred to the microscope.

### 3.3.4 Bacterial cytological profiling

BCP was performed to evaluate antibiotic effects on *B. subtilis* at two timepoints, 10 and 30 minutes, using the strain MW54, that expresses cytosolic GFP protein from a strong constitutive promotor (*PrpsD-gfp*). In addition, the dyes Nile red was used for membrane staining and DAPI for DNA staining [39] [46].

As illustrated in *Figure 5,* overnight cultures were first diluted in fresh medium and grown to mid-log phase ($OD_{600} \approx 0.30$). 100 µL aliquots were distributed into separate 2 mL plastic tubes, which were subsequently placed in a ThermoMixer set to 37 °C and 750 rpm. Antibiotics were added to each tube to final concentrations of 6.25 µM, 3.13 µM, and 1.56 µM Ru, 0.4 µg/mL nisin, and an untreated sample. The samples were then incubated in the dark for 10 and 30 minutes. For each time-set, seven minutes prior to imaging, Nile red (0.5 µg/mL) was added, followed by addition of DAPI (1 µg/mL) five minutes prior to imaging. Following the *3.3.3 Sample preparation* and using the dopamine coated coverslips, the prepared slide was imaged.

Imaging commenced immediately and all samples were imaged within 10 minutes. A minimum of three images per condition were captured using the pre-set phase contrast, RFP, GFP, and DAPI channels (see *Appendix C: Exposure settings*).

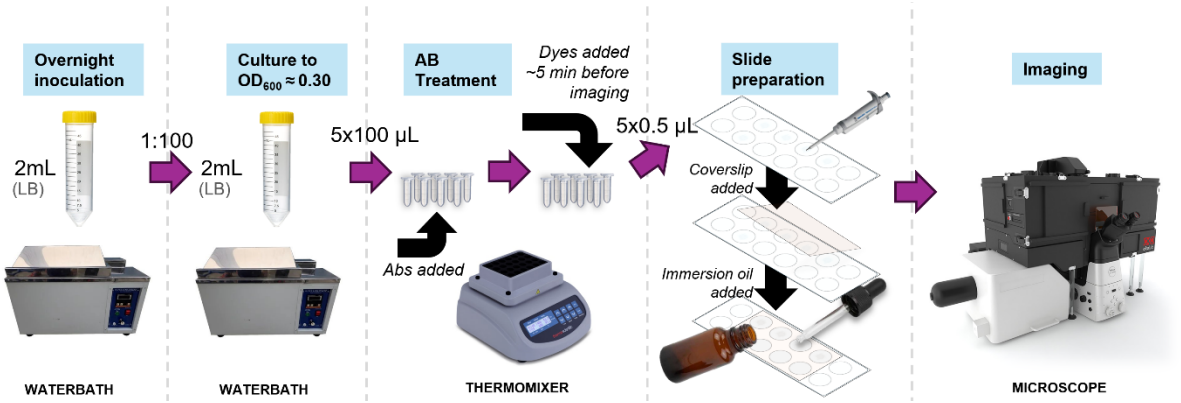


**Figure 5, Bacterial cytological profiling overview.** Every operation is segmented by instrument used with grey vertical lines and a light blue background title on top. Starting from left, the active culture volume is noted, and which media is used.

### 3.3.5 DNA Damage Assay

For the DNA-damage assay, the UG10 strain, which expresses a RecA-GFP fusion, was used to detect active DNA damage repair. . This strain requires culturing with added 0.5% Xylose as an inducer for the fusion protein expression and is thus cultured in LB media with added xylose. MitC was used as a positive control for DNA damage.

Overnight cultures of UG10 were diluted in fresh medium and grown to mid-log phase ($OD_{600} \approx 0.30$). Then, 100 µL aliquots were distributed into separate 2 mL plastic tubes, which were subsequently placed in a ThermoMixer set at 37 °C and 750 rpm. Antibiotics were added to each time-set of tubes to final concentrations of 6.25 µM, 3.13 µM, and 1.56 µM Ru, 0.05 µg/mL MitC, and an untreated sample. The samples were then incubated for 10 and 30 minutes in the dark. For each time-set, five minutes prior to imaging, DAPI (1 µg/mL) was added. Sample preparation was followed as described in *3.3.3 Sample*

Imaging for each time-set finished within 10 minutes from imaging start using specific instrument settings (see *Appendix C: Exposure settings)*.

### 3.3.6 Oxyburst microscopy

Oxyburst Green (Oxyburst) is a fluorescent dye which can be absorbed by bacteria to probe for the presence of ROS, mainly superoxide ions [29]. To evaluate oxidative stress, the wild type *B. subtilis* strain 168CA was imaged after a 30-minute antibiotic treatment time, using an adapted Oxyburst protocol [47]. The original protocol was adapted to work at 37 °C, requiring 160 minutes incubation with 10 µM Oxyburst prior to imaging. Samples were protected from light.

**Antibiotic treatment and culture handling**

Initially, an overnight 168CA strain culture was diluted 1:200 to a volume of 2 mL LB media with 0.2% glucose (LB**) with added 10 µM Oxyburst (*see Figure 6 for workflow*). Cell density was regularly monitored by $OD_{600}$ measurements and upon reaching $OD_{600} \approx 0.30$, the culture was aliquoted into four 2 mL plastic tubes with 200 µL culture each and was placed into a ThermoMixer (37 °C, 750 RPM). Antibiotics were added to each sample tube to final concentrations of Ru at 6.25 µM and 3.13 µM, $H_2O_2$ at 0.3% and a DMSO sample at 1%. The samples were then incubated for 30 minutes protected from light.

**PBS washing steps and microscopy imaging**

To reduce background fluorescence, the cultures were washed twice with PBS + 0.2% glucose (PBS**). This was done by centrifugation of the samples (30 s, 14 000 RPM), which were returned to the ThermoMixer (without shaking), and the LB** supernatant was removed. Cells were then resuspended in fresh 2 mL pre-warmed PBS** in each tube, vortexed, and again centrifuged (30 s, 14 000 RPM). The tubes were returned to the ThermoMixer, the PBS** supernatant removed, and cell pellets were resuspended in fresh 100 µL PBS** per tube, vortexed, and kept under agitation. Samples were prepared as described in *3.3.3 Sample preparation*

Imaging commenced immediately afterwards, and all samples were imaged within 10 minutes. A minimum of three images per condition were captured using the phase contrast and GFP channels (see *Appendix C: Exposure settings*).

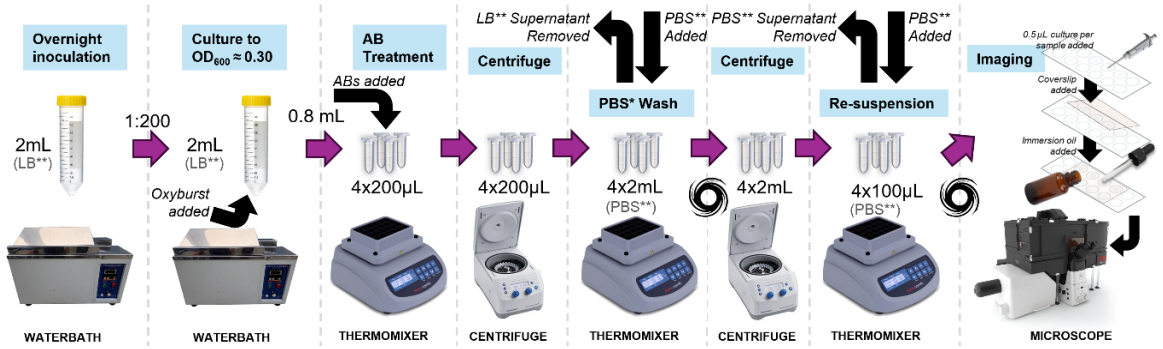


**Figure 6, Detailed Oxyburst assay workflow.** Each operation is segmented by instrument usage, clearly separated by vertical grey lines and titled with a light blue background. The figure indicates active culture volumes, vessels, instruments and additions/subtractions of liquid. The spiral circle symbols that samples were vortexed.

### 3.3.7 Image analysis

Following microscopy of the various assays, image analysis was performed using the Fiji/ImageJ software where segmentation and morphology-based analysis for the BCP and Oxyburst assays was conducted using the ObjectJ and MicrobeJ plugins using established methods [48][49][50]. Essentially, chains of bacteria were segmented and a minimum of 50 cells per condition per replicate were quantified. Example images of the use of these tools are explained in *Appendix B:Image Analysis.*

### 3.4 GFP Scavenger Spectroscopy

To evaluate the involvement of ROS in the previously observed Ru-induced protein degradation, a new assay was designed. To this end, *B. subtilis* MW54 (*PrpsD-gfp*) was grown in the presence of different ROS scavengers. The GFP signal was measured to assess protein degradation. . This GFP scavenger spectroscopy (GSS) assay uses mid-log phase ($OD_{600} \approx 0.30$) bacterial cultures exposed to Ru together with the ROS scavengers tiron (10 mM) and Thiourea (150 mM) [30][31]. The experimental design consisted of four distinct sets, a non-scavenger set, individual sets for each scavenger, and a combined scavenger set. Each set included three technical replicates per condition, a carrier control (blank) with PBS + 0.5% glucose (PBS*), untreated cell control (growth control), DMSO (1%), Ru at concentrations of 6.25 µM and 3.13 µM, and a positive control of $H_2O_2$ (0.3%) (*see Figure 7 for plate layout).* To minimize the delay between exposure initiation and start of measurement, the plate was pre-loaded with solutions containing double the final concentration of scavengers and antibiotics, thus allowing the addition of equal volumes of cell culture using a multichannel pipette.

| | 1 | 2 | 3 | 4 | 5 | 6 | 7 | 8 | 9 | 10 | 11 | 12 |
|---|---|---|---|---|---|---|---|---|---|---|---|---|
| A | PBS* | | | PBS* | | | PBS* | | | PBS* | | |
| B | Cells | | | Cells | | | Cells | | | Cells | | |
| C | DMSO | | | DMSO | | | DMSO | | | DMSO | | |
| D | Ru3 | | | Ru3 | | | Ru3 | | | Ru3 | | |
| E | Ru6 | | | Ru6 | | | Ru6 | | | Ru6 | | |
| F | Pt1 6 | | | Pt1 6 | | | Pt1 6 | | | Pt1 6 | | |
| G | H2O2 0.0096% | | | H2O2 0.0096% | | | H2O2 0.0096% | | | H2O2 0.0096% | | |
| H | H2O2 0.3% | | | H2O2 0.3% | | | H2O2 0.3% | | | H2O2 0.3% | | |
| | PBS* | | | Tiron | | | Thiourea | | | Tir+Thio | | |

**Figure 7**, **Overview of GSS assay plate layout.** Columns 1–3 (grey) represent the non-scavenger set, columns 4–6 (blue) represent the tiron set, columns 7–9 (orange) represent the thiourea set, and columns 10–12 (blue and orange) represent the combined tiron and thiourea set. Each cell represents three technical replicates subjected to identical treatments.

#### Plate preparation

Prior to the bacterial culture reaching $OD_{600} \approx 0.30$, stock solutions for each scavenger set were prepared at twice the final scavenger concentration in PBS*. Approximately 30 minutes before the culture reached the target OD, 98 µL of these scavenger solutions were distributed into the respective wells (see *Figure 8*). Subsequently, 102 µL PBS* were added to row A and 2 µL additions of antibiotic stock solutions were made according to *Figure 8.* The plate was inspected to remove any bubbles and placed in the plate reader to pre-warm before sample addition.

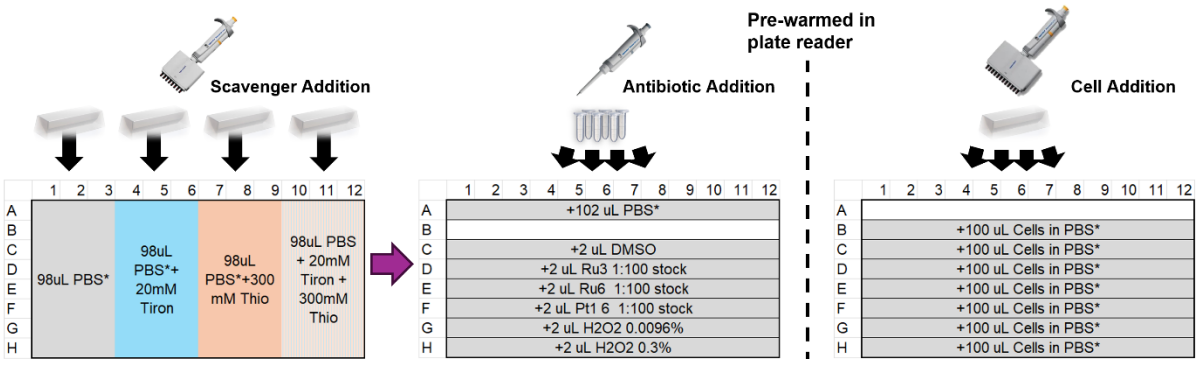


**Figure 8, GSS assay plate preparation workflow.** The left plate illustrates initial scavenger addition from reservoirs into the designated wells. The middle plate shows PBS* being added to row A and antibiotics to other rows, excluding row B, which was reserved for cells only. The right plate shows the final addition of cell suspension to the heated prepared plate stored in the plate reader until addition.

**Preparation of cells**

An overnight MW54 strain culture was diluted 1:100 in 20 mL fresh LB medium with 0.5% glucose (LB*) in a 100 mL culture flask (*see Figure 9 for workflow*). Cell density was regularly monitored by $OD_{600}$ measurements and upon reaching $OD_{600} \approx 0.30$, the culture was aliquoted into eight 2 mL plastic tubes and placed into a ThermoMixer set at 37 °C and 750 RPM. Cultures were washed with and resuspended in PBS* to bypass LB autofluorescence. This was done by transferring the tubes to be centrifuged (30 s, 14000 RPM), then returned to the ThermoMixer were the supernatant was carefully removed. Cells were resuspended in fresh, 1.8 mL pre-warmed PBS* added to each tube, vortexed and returned to the PBS* 50 mL Falcon tube. The cells in PBS* were then added to the pre-warmed plate and the measurement was started (*see Appendix C:GSS settings*). Post measurements, the plate reader GFP intensity data is analyzed with Microsoft Excel. For each respective set and timepoint the measured mean intensity of blank wells was used for baseline subtraction and a mean of the growth controls were used to normalize the GFP intensity for each set and timepoint.

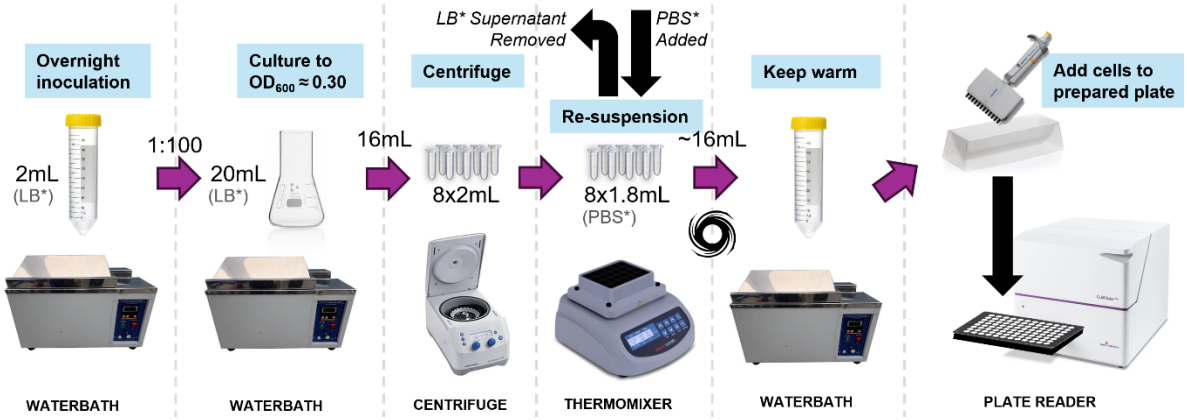


**Figure 9, Detailed scavenger assay workflow.** Each operation is segmented by instrument usage, clearly separated by vertical grey lines and titled with a light blue background. The figure indicates active culture volumes, vessels, instruments and additions/subtractions of liquid. The spiral circle symbols that samples were vortexed.

# 4. Results

## 4.1 MIC and OSC determination

At the beginning of this study a MIC assay was performed. This assay was used to determine the lowest concentration that inhibits bacterial growth. Ru had an MIC of 6.25 µM, nisin a MIC of 2 µg/ml, and the carrier DMSO impacted growth only at concentrations near 8% (v/v), diagrams can be found in *Appendix A:MIC.*

A subsequent growth curve was conducted based on the identified MIC concentrations and the results can be seen in *Figure 10*. Here, the purpose was to identify the OSC for both Ru and nisin. Studies with the antibiotic exposure at OSC allow mechanistic insight into how the antibiotic affects an organism before directly killing it. This concentration is defined to cause a 50-70% growth inhibition compared to an untreated growth control in exponential growth phase (*see Appendix B: OSC*). For Ru, the OSC was 3.125 µM and for nisin was between 0.2 and 0.4 µg/mL.

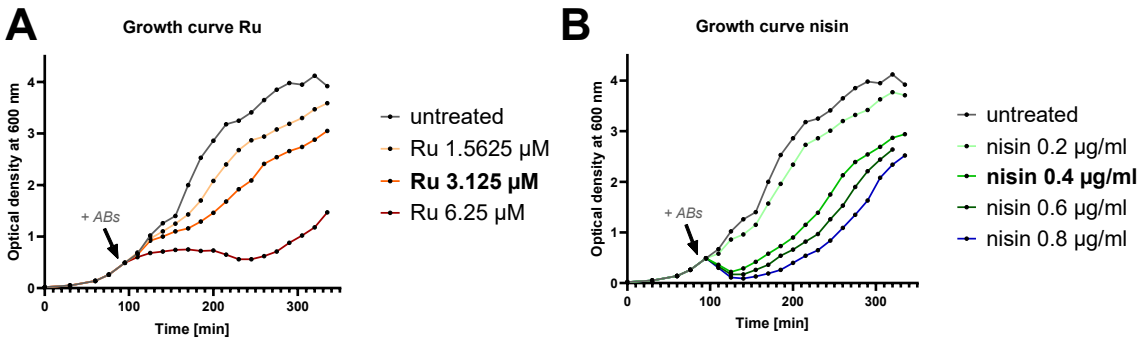


**Figure 10, growth curves for Ru and nisin treatments.** In both A and B, measurement points are represented by black dots on lines. Different line colors indicate different compound concentrations, which can be found in the legend. After 95 min of initial growth, the antibiotics were added and effects recorded for following 240 min. The left (A) shows a growth curve of Ru, while the right shows a growth curve of nisin. Identified MIC and OSC are marked in bold.

## 4.2 Bacterial cytological profiling

After determining the MIC and OSC, the effect of Ru on *B. subtilis* MW54 (*PrpsD-gfp*) cells was assessed using bacterial cytological profiling. Samples were prepared with an untreated control, a nisin-treated positive control, and to investigate concentration-dependent effects of Ru the established MIC and OSC concentrations were included. Treatments were applied for 10 and 30 minutes and imaged in two biological replicates (see *Appendix A:BCP* for second replicate). Representative cells are shown in *Figure 11*,

Untreated control samples show successful staining across all fluorescent channels, the NR membrane stain appeared evenly distributed along the bacterial membrane. Occasional foci overlapping the width of the chain can be seen which corresponds to division septa as seen in the NR channel for the untreated cells at 30 minutes (*Figure 11*). At certain stages of growth septa are visible in the phase contrast as slight constrictions that often co-localize with a lower intensity in the GFP signal also often visible at septa locations. The DAPI staining shows clearly defined, symmetrical, and relaxed chromosomal DNA packages implying normal unimpaired cell division.

Upon exposure to increasing concentrations of Ru, additional foci distinct from septal formation can be observed in the membrane stain. These foci are indicative of membrane altercations, for example, fluid domains, invaginations, or intracellular vesicles. The domains with higher fluidity are less densely packed, which in turn can enable more dye molecules like the NR to bind into the membrane [51]. Membrane invaginations and intracellular vesicles both produce higher dye intensities due to superimposed extra bilayer material [52]. These altercations are stress-related and suggest that Ru treatment causes membrane stress. This effect is particularly apparent in the positive control for membrane stress of nisin treated cells subjected to strong membrane disruption by pore formation.

The cytosolic GFP signal, which appeared uniformly distributed, exhibited a clear concentration-dependent reduction in fluorescence intensity following Ru treatment. This observation aligns with findings that showed general protein degradation. As previously conducted assays showed no pore-forming activity (*propidium iodide* and *DiSC$_3$(5)* assays), this could suggest that Ru exposure induces proteolytic activity. Moreover, Ru-treated samples show signs of uneven DNA distribution and packing compared to the symmetrical DNA packages in untreated cells, implying possible DNA damage.

All mentioned cytological effects such as the apparent membrane stress, reduction of GFP signal intensity, and DNA distribution alterations were consistently observed across two biological replicates. In summary, the proteins, the lipid membrane, and the DNA appear to be affected by the Ru complex. This type of diverse damage is common for how oxidative stress impairs organisms. These findings could therefore also indicate induction of oxidative stress by Ru, which aligns with *hypotheses 4*.

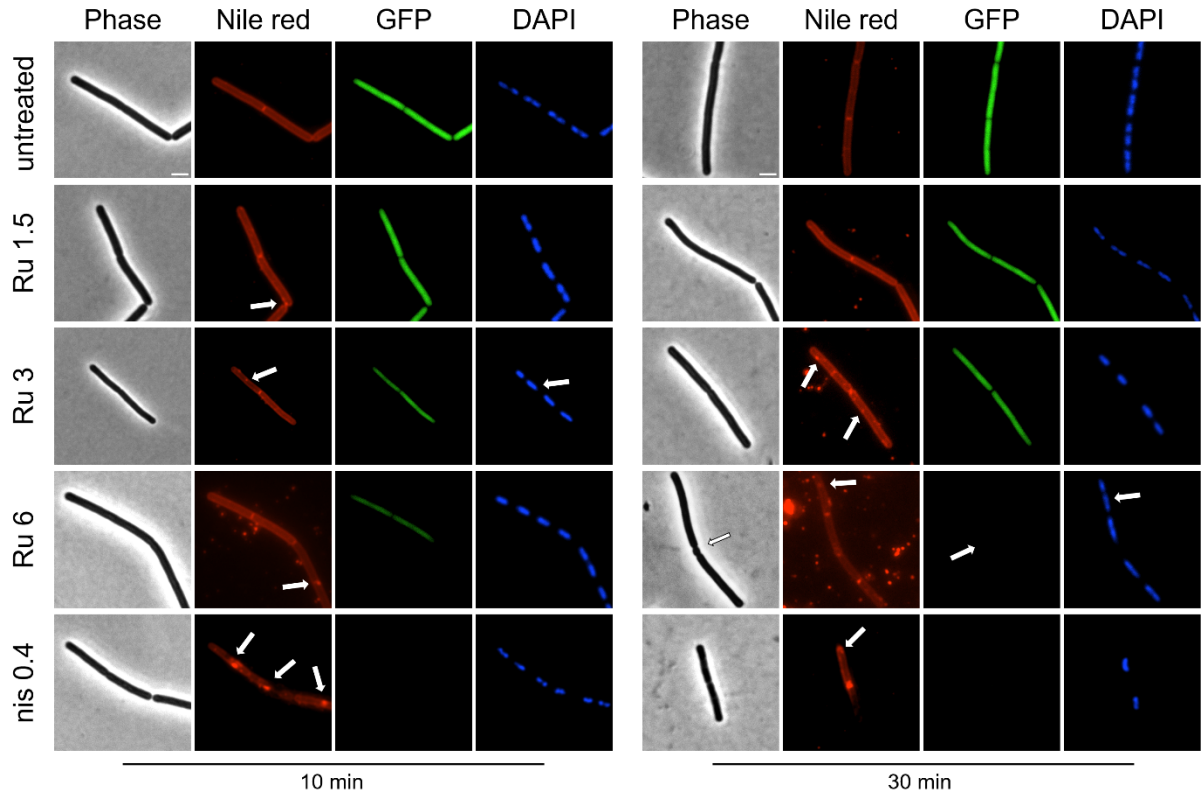


**Figure 11, Bacterial Cytological Profiling (BCP).** *B. subtilis* strain MW54 (*PrpsD-gfp*) treated for 10 and 30 minutes with Ru at concentrations of 1.5625 (1.5), 3.125 (3), and 6.25 µM (6), alongside a positive control of nisin (nis) at 0.4 µg/mL and an untreated sample. The GFP channel's brightness and contrast are scaled equally. Scale bar represents 2 µm. Arrows in Nile red point to membrane stress foci and in the DAPI at unevenly packed DNA.

### 4.2.1 Membrane stress

The bacterial cytological profiling indicated that Ru causes membrane stress. To quantify the extent of membrane stress, image analysis was performed, cell chains were segmented at septa into individual cells, counted as either stressed (cells with distinct membrane foci) or normal (cells exhibiting evenly distributed membrane staining). At least 50 cells per sample across two biological replicates were analyzed. The percentage of stressed cells relative to the total cell count per sample is presented in *Figure 12A*. Indeed, treatment with Ru significantly increased membrane stress compared to the untreated control. However, a notable increase of intercellular foci in the NR staining was consistently observed in samples exposed to higher Ru concentrations (*Figure 12B*). This increase in intercellular foci interfered with the identification of membrane foci, which is why the quantification of membrane stress for these samples (light grey bars, *Figure 12A*) must be interpreted cautiously.

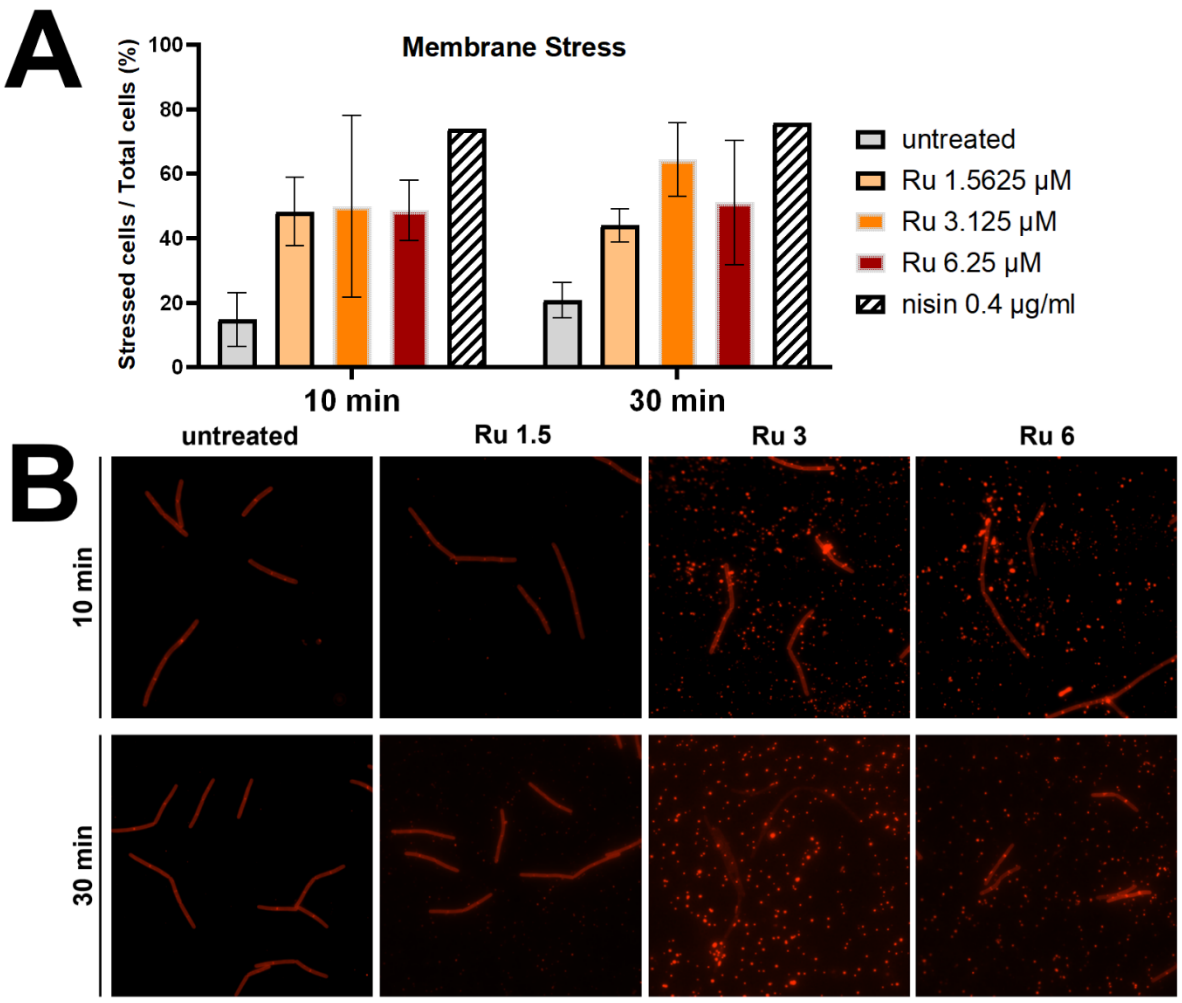


**Figure 12, Relative membrane stress and Nile-red intercellular foci.** Percentage of *B. subtilis* MW54 (*PrpsD-gfp*) cells exhibiting membrane stress (A) and overview of the Nile red stain for different Ru concentrations (B).

### 4.2.2 Loss of GFP signal

Another striking phenotype of Ru treatment in the BCP was the loss of GFP signal. Previous studies have shown that Ru is not a pore former like the nisin positive control, which indicates that other processes are involved. Here, the GFP intensity was quantified in individual cells. Individual bacteria were resolved from chains, analyzed, and quantified for mean GFP intensity. The quantified intensities from the two biological replicates are compiled for each treatment timepoint into *Figure 13*. It was observed that the treatments caused an obvious reduction in the GFP intensity and that this effect appeared dependent on both concentration and treatment time

Statistical comparison of pooled data for Ru-treated samples against the untreated control confirmed highly significant reductions in the GFP signal (**** = adjusted $P < 0.0001$, one-way ANOVA with Dunnett's post-test). These statistical significance is the same for the separate biological replicates that can be seen in *Appendix A: BCP-GFP*. After 10 min, fluorescence fell by 7%, 30% and 55% at 1.5625, 3.125 and 6.25 µM Ru, respectively and extending the treatment to 30 min further caused decreases to 13%, 40% and 68%.

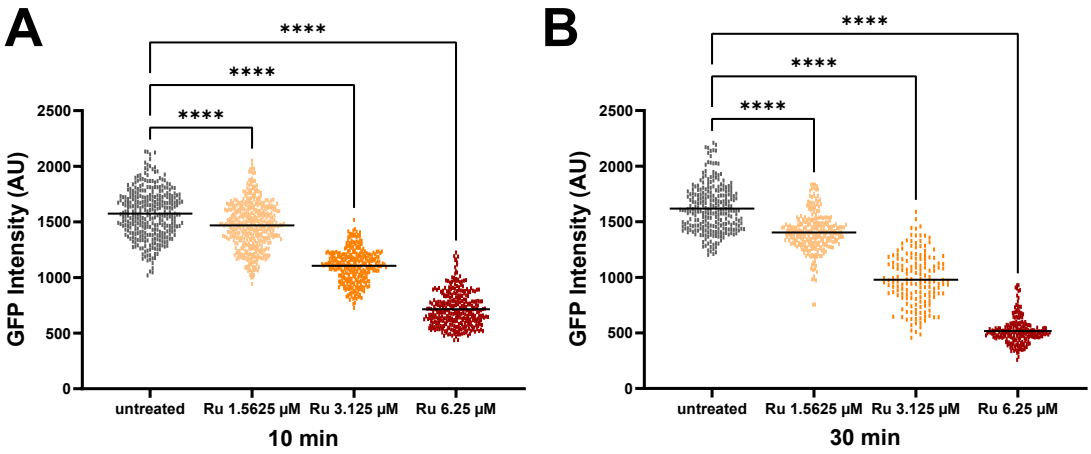


**Figure 13, GFP intensity after Ru treatment.** Scatter plots of pooled GFP intensity data from two biological replicates of *B. subtilis* MW54 (*PrpsD-gfp*) measured after 10 min (A) and 30 min (B) exposure to Ru (1.5625 µM, 3.125 µM, 6.25 µM) compared with an untreated control. Asterisks denote significance (****, $P < 0.0001$). Black horizontal bars indicate group means. One-way ANOVA with Dunnett's post-test versus the untreated control; confidence intervals (95 %) of mean AU differences: (A) untreated vs Ru 1.5625 µM = 74-139, untreated vs Ru 3.125 µM = 435-504, untreated vs Ru 6.25 µM = 825-894; (B) untreated vs Ru 1.5625 µM = 178-252, untreated vs Ru 3.125 µM = 597-684, untreated vs Ru 6.25 µM = 1062-1141.

### 4.3 DNA Damage Assay

BCP revealed changes in DNA compaction. To follow up on this observation, *B. subtilis* strain UG10 expressing the RecA-GFP fusion was used to assess DNA damage induced by Ru exposure. As RecA is a repair protein recruited to single-stranded DNA regions, a clustering of RecA on the DNA is indicative of DNA damage. Images of representative cells after 10- and 30-minutes of treatment with increasing concentrations and a positive control are presented in *Figure 14*.

The RecA–GFP fluorescence was evenly distributed in the untreated samples at both time points indicating that treatment with 1% DMSO alone does not induce a visible DNA damage response. Exposure with Ru induced distinct RecA–GFP foci on the DAPI-stained nucleoids. At the low and mid Ru concentrations, there were visible RecA foci that appeared more intense with higher concentration. The bright RecA-GFP foci observed at both time points for all tested Ru concentrations as well as for the MitC positive control, indicate RecA recruitment to damaged sites with single-stranded DNA. RecA evaluation of the highest Ru concentration was however more difficult due to the loss of GFP signal that is likely due to Ru-induced proteolysis (*Section 4.2*). This signal reduction affects accurate visualization of the reporter and may represent a threshold, for which fluorescence-based assays become unreliable for studying this antibiotic.

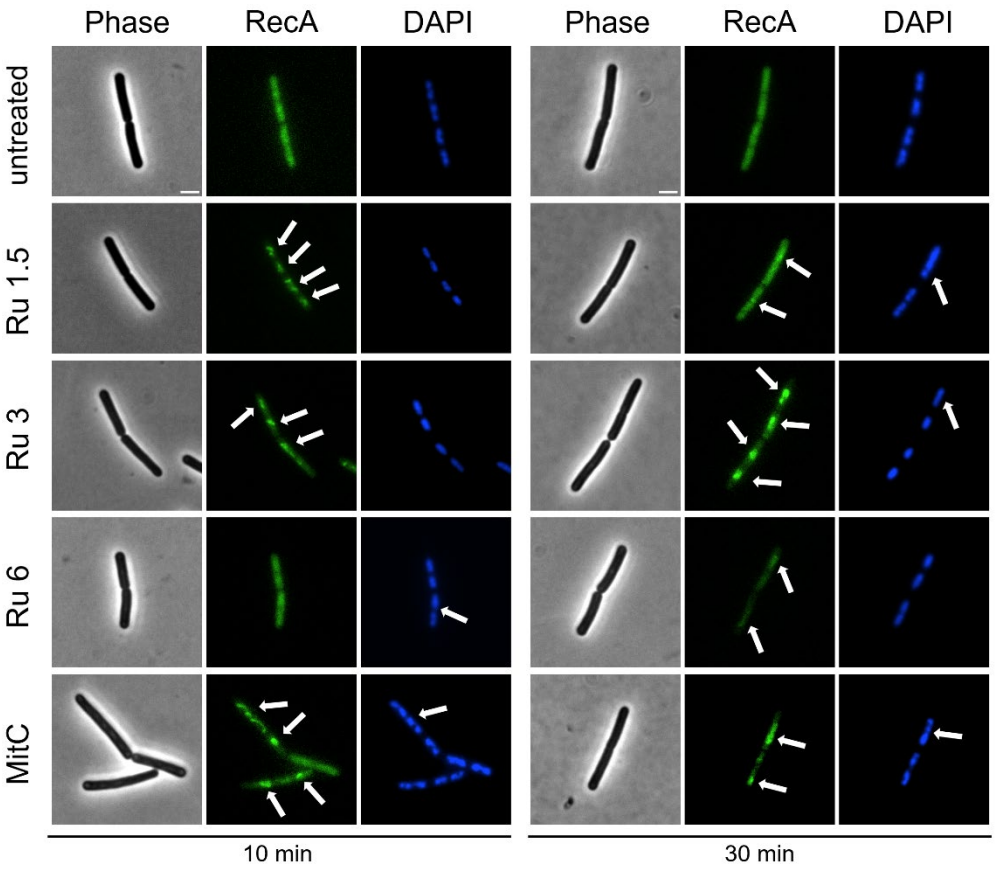


**Figure 14, RecA-GFP response to Ru-induced DNA damage.** *B. subtilis* strain UG10 (*amyE::Pxyl-recA-mgfp* spc) treated for 10 and 30 minutes with Ru at concentrations of 1.5625 (1.5), 3.125 (3), and 6.25 µM (6), alongside a positive control of mitomycin C (MitC) at 0.05 µg/mL and an untreated sample. Untreated cells exhibit diffuse GFP, whereas Ru and mitomycin C display discrete GFP foci marked with arrows. Arrows in DAPI point to DNA symmetry abnormalities. Scale bar represents 2 µm.

### 4.4 Oxyburst assay

Imaging with Oxyburst was conducted to see if DNA damage may be caused by ROS. Oxyburst is a fluorescent probe for the presence of superoxide radicals. Here, Oxyburst was measured in cells treated with increasing concentrations of Ru and $H_2O_2$ as a positive control. Using the phase contrast as a guide to aid bacterial chain segmentation, mean intensities of at least 50 comparable smaller chains per condition were quantified. Three biological replicates of these mean intensities were pooled and presented in *Figure 15* (see *Appendix A:Oxyburst* for individual biological replicates).

Analysis of the pooled fluorescence intensities revealed uniform distributions with low variance in both the DMSO control, and the Ru treated samples. The 1% DMSO carrier control had a mean fluorescence intensity of 500 AU, which is higher than the background (mean ≈ 300 AU). This is expected and likely due to inherent normal levels of cytosolic ROS in the bacteria.

Statistical comparison of pooled data for Ru and $H_2O_2$ treatments against the DMSO control demonstrated significant differences at a 1- to 4-sigma confidence level (between * and **** = adjusted $P < 0.05$ and 0.0001, one-way ANOVA with Dunnett's post-test versus 1% DMSO), see *Appendix A: Oxyburst* for the individual biological replicate significances, comparison between untreated and Ru 1.5 had a lower level of significance. Following baseline correction by subtracting the background fluorescence, the 0.3% $H_2O_2$ treatment showed an increased fluorescence intensity of approximately 70% while the Ru treatments displayed a dose-dependent reduction in fluorescence with a decrease by 10% at 3.125 µM and by 42.5% at 6.25 µM relative to the carrier control.

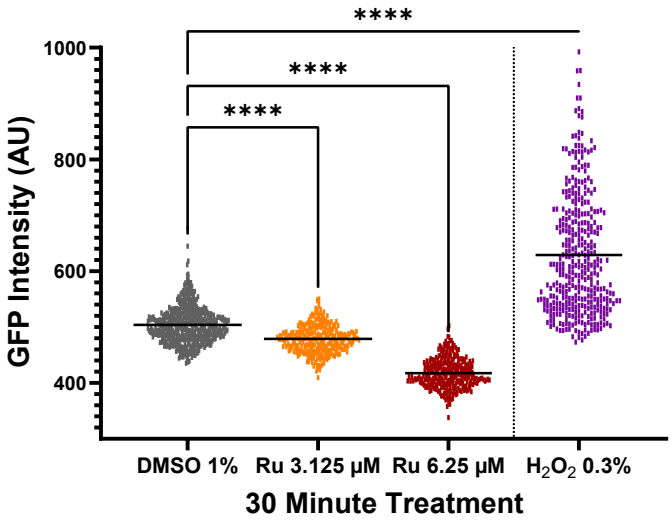


**Figure 15. Intracellular superoxide presence after 30 min antibiotic treatment.** Scatter plots of Oxyburst fluorescence in *B. subtilis* for treatment with Ru (3.125 µM, 6.25 µM), 1% DMSO, and 0.3% $H_2O_2$. Asterisks indicate ANOVA significance. Black horizontal bars show the group mean intensities. One-way ANOVA with Dunnett's post-test versus 1% DMSO with confidence intervals (95%) of mean AU differences: DMSO vs Ru 3.125 µM = 15-35, DMSO vs Ru 6.25 µM = 77-96, DMSO vs $H_2O_2$ 0.3 % = -134 to -116.

### 4.5 GFP scavenger spectroscopy

To further understand the role of ROS, a GFP spectroscopy assay with different ROS scavengers, which counteract either superoxide or hydroxyl radicals, was conducted. Here, different concentrations of Ru were tested along samples treated with 0.3% $H_2O_2$ as positive control, DMSO as carrier control, untreated cells as growth control, and media blanks for baseline intensities. Baseline-corrected and normalized GFP intensities of this assay with different scavenger sets can be seen for the 30-minute timepoint presented in *Figure 16* and kinetic plots of 0-35 minutes in *Figure 17*. Two additional biological replicates that show similar characteristics can be found in *Appendix A: GSS.*

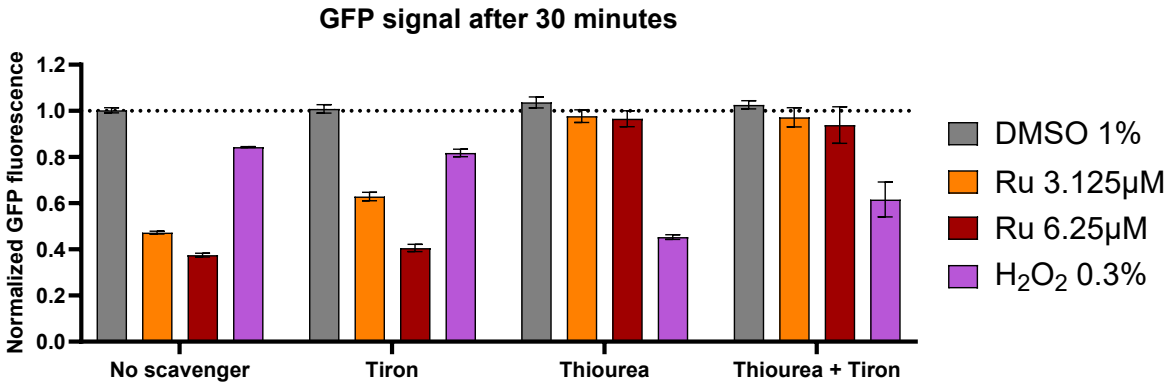


**Figure 16, GFP content after 30 minutes of antibiotic treatment in the presence of scavengers.** The value of the normalized GFP fluorescence intensity from three technical replicates of *B. subtilis* MW54 after 30 min. Dotted line represents normalized GFP signal of the untreated control.

In the absence of scavengers, both Ru concentrations induced a GFP fluorescence reduction consistent with the previous BCP results. GFP levels for DMSO-treated cells remained stable, while the 0.3% $H_2O_2$ positive control displayed some fluorescence decrease. This set confirmed the suitability of the assay to measure Ru-induced protein degradation.

In the presence of 10 mM tiron, which mainly scavenges superoxide radicals, the fluorescence profiles are similar to the set without scavengers, indicating minimal involvement of superoxide in the Ru MoA. Little to no effect was observed for the positive control with the tiron scavenger. $H_2O_2$ is a hydroxyl radical donor, thus tiron is not expected to reduce its effects.

In the set of 150 mM thiourea, known to neutralize hydroxyl radicals and $H_2O_2$, the GFP fluorescence across both Ru treatments is extraordinarily well preserved compared to the GFP in the set with no scavengers. This preservation also can be seen in the kinetic data where there is an initial GFP decrease which then recovers as seen in *figure 17C*. This GFP preservation suggests that a major factor of what makes the Ru induce protein degradation, thus becoming antimicrobial, is the induction of hydroxyl radicals. In this set the $H_2O_2$ positive control on the contrary causes severe GFP degradation with the thiourea which suggests that the positive control concentration used here was too high for the scavenger to alleviate its effects.

The combined thiourea and tiron set show similar GFP effect from Ru-treated cultures to the thiourea set alone. If compared to the set with only thiourea the tiron appears to decrease the effect where the thiourea and $H_2O_2$ caused a severe GFP intensity decrease.

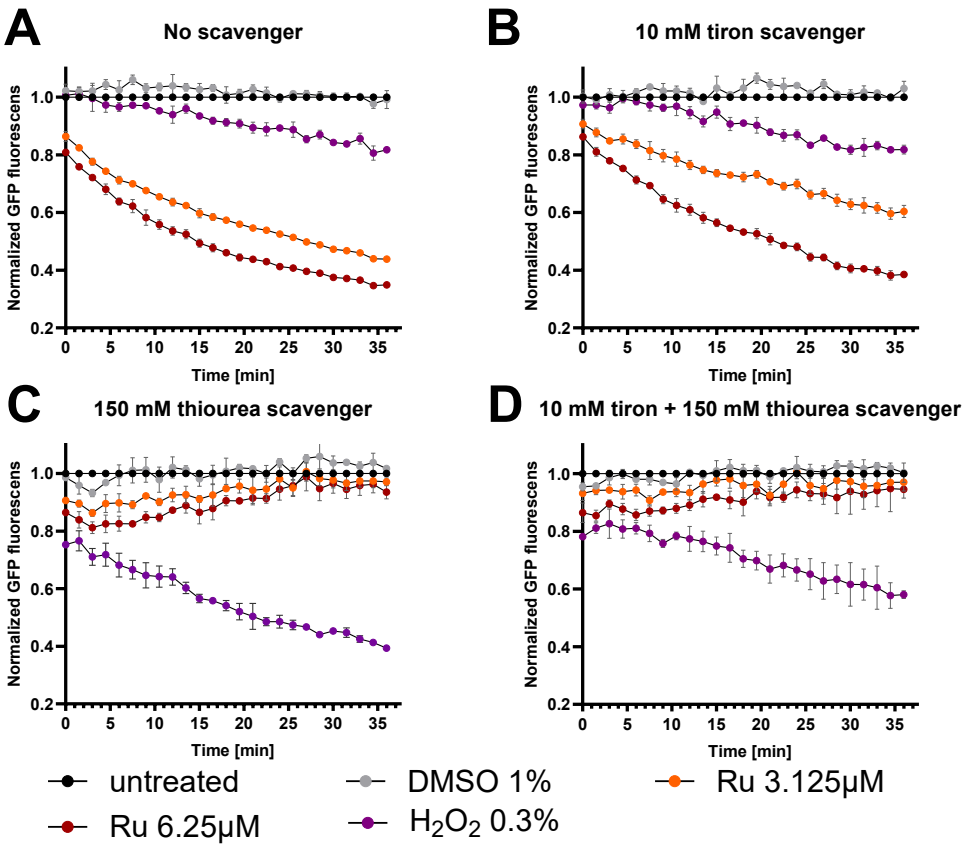


**Figure 17, GFP scavenger spectroscopy results.** Normalized GFP fluorescence intensity from three technical replicates of *B. subtilis* MW54 cultures. GFP signal was monitored every 90 seconds for 35 min after addition of cell cultures to a pre-prepared plate with antibiotics: no scavenger (A), 10 mM tiron (B) that targets $O_2^{\bullet -}$, 150 mM thiourea (C) that neutralizes OH• and the combined set with both thiourea and tiron (D).

Identified by the scavenger specificity of thiourea, the short-lived hydroxyl radicals seem to be particularly involved in the Ru-induced proteolysis. Ru likely has a catalytic role in the conversion of $H_2O_2$ into highly reactive hydroxyl radicals much like how iron ions mediate Fenton reactions to generate hydroxyl radicals [53]. In the Oxyburst tests, an unexplained decrease in the superoxide concentration was observed. As Ru likely causes catalysis of $H_2O_2$ to hydroxyl radicals, this could effectively deplete cytosolic $H_2O_2$. In turn, this could shift an equilibrium where more superoxide radicals convert into $H_2O_2$. Alternatively, the Ru compound itself might be able to catalyze the superoxide conversion further depleting the superoxide ions, which would explain the Oxyburst results.

## 5. Discussion

The findings presented here strongly support the hypothesis that oxidative stress mediates protein degradation as the primary MoA for Ru. It is important to note that antibiotics can have multiple MoA, and the initial other hypotheses involving direct protease activation or protein misfolding are not disproven by these findings. However, given that previous experiments with cytosolic protease knockout strains showed minimal impact on Ru activity, a protease-dependent mechanism now seems unlikely. A plausible alternative theory to be tested is that the Ru could exhibit a direct protein-destroying effect.

An interesting finding was the observed intercellular foci in the NR from the BCP assay. These remain unexplained but identified in many samples to increase with Ru concentration and treatment time. Two plausible explanations are that the foci may be attributed to either small membrane vesicles forming or direct NR-Ru interactions causing some sort of precipitation. Small membrane vesicles have lipid bilayers close together which could explain the elevated NR intensity.

The experiments consistently demonstrated diverse protein degradation, distinct membrane stress and DNA damage repair activation. The combination of these types of damage are hallmarks of oxidative damage. The decrease in the GFP intensity as reporter for protein degradation, is however very rapid and pronounced compared to conventional antibiotics. It would therefore be interesting to determine the cause of this with further assays. Further insights from transcriptomics also revealed upregulation of both oxidative stress responses and protein stress responses that support the oxidative stress hypothesis (*M. Wenzel, unpublished*).

The observed decrease in fluorescence in the Oxyburst assay suggests that Ru effectively reduces intracellular superoxide concentrations. While this result initially may appear inconsistent with oxidative stress mediated protein degradation, it is important to consider the broader biological ROS balance. Intracellular ROS levels are connected and regulated by enzymatic equilibria, and organometallic complexes such as Ru are well-known for their catalytic capabilities in reactions [54]. This suggests that perhaps Ru catalyzes superoxide conversion to $H_2O_2$ and then to hydroxyl radicals.

Reflecting on the experimental design, the use of $H_2O_2$ as a positive control could be reconsidered as it is not explicitly known to elevate superoxide levels. However, in the results it was observed that $H_2O_2$ increases the fluorescence intensity relative to the carrier control that indicates a rise in superoxide concentration by the $H_2O_2$. Alternatively, and perhaps more likely, this could be due to a lower specificity for superoxides of the probe than what the company claims.

Post interpretation, it was also found that these mechanistic insights align closely with findings from *Weng et al*., who also report bactericidal effects of organoruthenium complexes on G (+) bacteria driven by induction of ROS [55]. Their work also showed how thiourea as a scavenger could be used to effectively quench the bactericidal effects of the organoruthenium complexes.

## 5.1 Proposed mode of action

The interpretation of the results across all assays suggests that Ru induces membrane stress, GFP degradation, and DNA damage. The GSS suggests ROS involvement, in which the scavenging specificity of thiourea for hydroxyl radicals appears to inhibit the protein degradation effect. This in turn suggests that Ru induces hydroxyl radicals as a potential MoA.

As illustrated in *Figure 18,* the current working model is that Ru catalyzes cytosolic superoxide and $H_2O_2$ reserves into hydroxyl radicals, which in turn cause disruptive oxidative damage to DNA, lipids, and proteins. Cytosolic proteases likely recognize these damaged and misfolded proteins and degrade them, which further accelerates proteolytic activity resulting in proteome-wide protein breakdown. This MoA explains the observed damage including the increased protein degradation seen reduced in the GFP content.

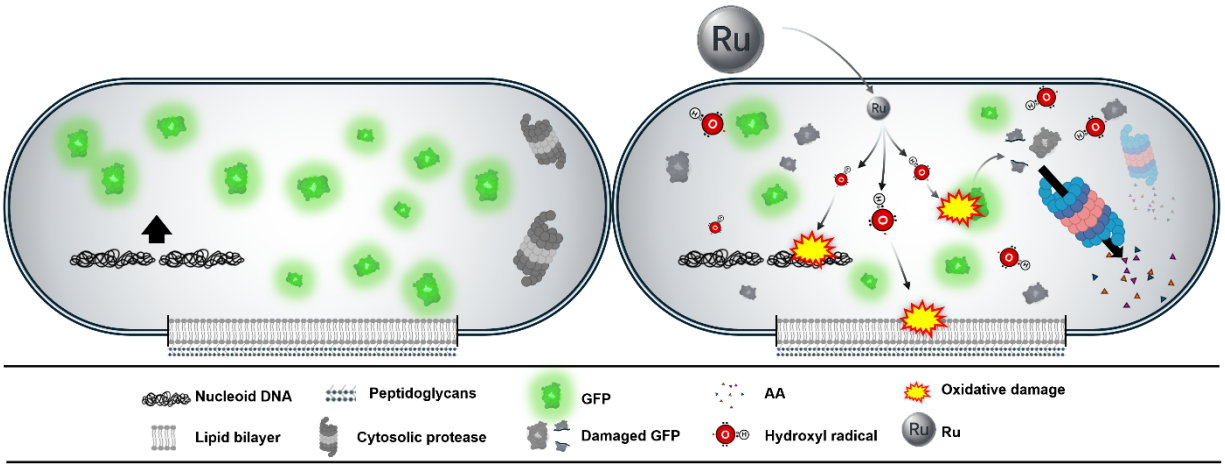


**Figure 18. Proposed mode of action of Ru in GFP-expressing *B. subtilis*.** Unaffected bacterium with normal function and cytosolic GFP (left), and a bacterium subject to Ru exposure (right). Ru structure is for illustrative purposes and not scientifically accurate.

## 5.2 Outlooks

To further investigate these intercellular foci in the NR, a simple experiment with the BCP method treating NR with Ru but without cells could be employed to rule out the foci from precipitation hypothesis. The other hypothesis that the intercellular foci arise from membrane structures could be tested by using alternative membrane dyes such as the *FM™ 4-64 red* or *FM™ 1-43 green* dyes. While the effect is already reproducible with NR, reproducing the effect with these FM dyes would provide stronger evidence that the observed foci arise from membranes rather than some Ru-dye interaction. To further investigate the membrane structures methods such as Laurdan microscopy for membrane fluidity or structured illumination microscopy for a higher resolution imaging could then be tested. Cryo-electron microscopy (cryo-EM) could perhaps also be used to confirm and characterize intra- and intercellular vesicle formation induced by Ru treatment.

The observed effects of the Ru treatments could be additionally verified by an experiment to rule out direct interaction between the Oxyburst dye and Ru. As a plate reader fluorescence spectroscopy experiment, replicates with wells containing different combinations of Oxyburst with $H_2O_2$ and Ru could clarify this. Additional tests with other fluorescent probes like *CellROX Green reagent* with claimed specificity to detect hydroxyl radicals [29], could be done to confirm if Ru catalyzes the conversion of $H_2O_2$ to produce the hydroxyl radicals.

Finally, to rule out alternative MoA and provide a solid basis for a mechanistic understanding of the antibacterial activity some additional experiments are proposed. These are centered at further confirmation of the hydroxyl radical hypothesis and to further assess if protease activity is changed with Ru treatment. In the following, these experiments are proposed, where test experiment specification (T), experiment hypothesis (H), and expected outcome that would support the hypothesis (E) is presented.

**T: SDS-PAGE assay repeated with thiourea**
H: Thiourea can protect against Ru-induced protein degradation
E: SDS-PAGE would show a (more) intact proteome

**T: Lipid peroxidation probe assay with Ru**
H: Membrane stress induced by Ru is caused by lipid peroxidation through elevated ROS
E: The probe shows an increase of lipid peroxidation in Ru-treated samples

**T: Spectroscopy of cell lysate with Ru**
H: Ru causes protein degradation through activation of protease-related promoters
E: The spectroscopy shows lower or no Ru effects (genes not expressed in lysates)

**T: Spectroscopy of just GFP with Ru**
H: Ru causes direct protein damage
E: The spectroscopy shows effects on the GFP with Ru

**T: GFP spectroscopy with Ru addition post $H_2O_2$ treatment**
H: Ru causes higher protein degradation through $H_2O_2$ catalysis to hydroxyl radicals
E: The spectroscopy shows a synergistically significantly higher GFP reduction compared to only Ru or $H_2O_2$ treated samples.

## 6. Conclusion

The present findings on the antibacterial action of Ru on *B. subtilis* suggest a complex oxidative mechanism where significant ROS generation leads to cell damage. ROS is generally known to cause indiscriminate macromolecular damage through DNA strand breaks, oxidation of membrane lipids, and of amino acids in proteins. The cytological assay in this study measured significant disruptions of membrane integrity, a strong GFP fluorescence reduction and indications of DNA damage. The GFP tagged DNA damage repair proteins showed that Ru induces DNA damage. The superoxide probe indicated that the compound caused a significant decrease in the superoxide concentration within bacterial cells. Finally, an assay using different scavengers provided strong indications that oxidative stress due to hydroxyl radicals rather than superoxide radicals are key mediators of the oxidative damage. To validate these findings, further experiments focused on ROS as well as experiments with proteases could be conducted that soon likely would culminate in a final mechanism of action for Ru.

## 7. References


[1]
Williams KJ. The introduction of 'chemotherapy' using arsphenamine - the first magic bullet. J R Soc Med. 2009 Aug;102(8):343-8. PMID: 19679737; PMCID: PMC2726818. https://doi.org/10.1258/jrsm.2009.09k036

[2]
Lucaciu, R.L.; Hangan, A.C.; Sevastre, B.; Oprean, L.S. Metallo-Drugs in Cancer Therapy: Past, Present and Future. *Molecules* 2022, *27*, 6485. https://doi.org/10.3390/molecules27196485

[3]
Marcelino PRF, Moreira MB, Lacerda TM, da Silva SS. Metal-Based Drugs for Treatment of Malaria. Biomedical Applications of Metals. 2017 Dec 30:167–93. PMCID: PMC7122828. https://doi.org/10.1007/978-3-319-74814-6_8

[4]
Jessica E Waters et al, Recent advances in the development of metal complexes as antibacterial agents with metal-specific modes of action, *Current Opinion in Microbiology*,Volume 75, 2023, 102347, ISSN 1369-5274, https://doi.org/10.1016/j.mib.2023.102347

[5]
Özsan, Ç.; Schäfer, A.-B.; Akhir, A.; Aning, O.A.; Fulgencio, S.; Maitra, R.; Rani, R.; Saxena, D.; Westerlund, F.; Chopra, S.; Wenzel, M.; Frei, A. *A Platinum Butterfly Effect: Small Changes Turn an Anticancer Drug into a Non-toxic Metalloantibiotic with In Vivo Efficacy*. bioRxiv 2025, preprint 2025.05.30.657029v1. https://doi.org/10.1101/2025.05.30.657029

[6]
Fulgencio, S.; Scaccaglia, M.; Frei, A. Exploration of Rhenium Bisquinoline Tricarbonyl Complexes for their Antibacterial Properties. *ChemBioChem* 2024, *25*, e202400435. https://doi.org/10.1002/cbic.202400435

[7]
Evans, A.; Kavanagh, K.A. Evaluation of metal-based antimicrobial compounds for the treatment of bacterial pathogens. *Journal of Medical Microbiology* 2021, *70* (5). https://doi.org/10.1099/jmm.0.001363

[8]
Frei, A.; Zuegg, J.; Elliott, A.G.; Baker, M.; Bräse, S.; Brown, C.; Chen, F.; Dowson, C.G.; Dujardin, G.; Jung, N.; King, A.P.; Mansour, A.M.; Massi, M.; Moat, J.; Mohamed, H.A.; Renfrew, A.K.; Rutledge, P.J.; Sadler, P.J.; Todd, M.H.; Willans, C.E.; Wilson, J.J.; Cooper, M.A.; Blaskovich, M.A.T. Metal complexes as a promising source for new antibiotics. *Chem. Sci.* 2020, *11*(10), 2627–2639. https://doi.org/10.1039/C9SC06460E

[9]
Errington J, Aart LTV. Microbe Profile: *Bacillus subtilis*: model organism for cellular development, and industrial workhorse. Microbiology (Reading). 2020 May;166(5):425-427. Epub 2020 May 4. PMID: 32391747; PMCID: PMC7376258. https://doi.org/10.1099/mic.0.000922

[10]
J Heimbach LLC, GRAS Notice No. 956: *Bacillus subtilis* PLSSC (ATCC SD 7280), U.S. Food and Drug Administration, 2020. https://www.fda.gov/media/146998/download

[11]
Pedreira, T.; Elfmann, C.; Stülke, J. The Current State of SubtiWiki, the Database for the Model Organism *Bacillus subtilis*. *Nucleic Acids Res.* 2022, 50 (D1), D875 – D882. https://doi.org/10.1093/nar/gkab943

[12]
Stülke, J.; Grüppen, A.; Bramkamp, M.; Pelzer, S. *Bacillus subtilis, a Swiss Army Knife in Science and Biotechnology*. J. Bacteriol. 2023, 205, e00102-23. https://doi.org/10.1128/jb.00102-23

[13]
Tiago Pedreira, Christoph Elfmann, Jörg Stülke, The current state of *Subti*Wiki, the database for the model organism *Bacillus subtilis*, *Nucleic Acids Research*, Volume 50, Issue D1, 7 January 2022, Pages D875–D882, https://doi.org/10.1093/nar/gkab943

[14]
Gutsmann, T.; Seydel, U. Impact of the glycostructure of amphiphilic membrane components on the function of the outer membrane of Gram-negative bacteria as a matrix for incorporated channels and a target for antimicrobial peptides or proteins. *European Journal of Cell Biology* 2010, *89*(1), 11–23. https://doi.org/10.1016/j.ejcb.2009.10.011

[15]
Tetteh, J.N.A.; Matthäus, F.; Hernandez-Vargas, E.A. A survey of within-host and between-hosts modelling for antibiotic resistance. *Biosystems* 2020, *196*, 104182. https://doi.org/10.1016/j.biosystems.2020.104182

[16]
J. Errington and L. T. van Aart, “Microbe Profile: *Bacillus subtilis*: model organism for cellular development, and industrial workhorse,” *Microbiology*, vol. 166, pp. 425–427, 2020. https://doi.org/10.1099/mic.0.000922.

[17]
Y. Chai, R. Kolter and R. Losick, “Reversal of an epigenetic switch governing cell chaining in *Bacillus subtilis* by protein instability,” *Molecular Microbiology*, vol. 78, pp. 218–229, 2010. https://doi.org/10.1111/j.1365-2958.2010.07335.x.

[18]
J. H. Hageman *et al.*, “Single, chemically defined sporulation medium for *Bacillus subtilis*: growth, sporulation, and extracellular protease production,” *J. Bacteriol.*, vol. 160, pp. 438–441, 1984. https://doi.org/10.1128/jb.160.1.438-441.1984.

[19]
C. López-Otín and J. S. Bond, "Proteases: Multifunctional Enzymes in Life and Disease," *J. Biol. Chem.*, vol. 283, no. 45, pp. 30433–30437, 2008. [Online]. Available: https://doi.org/10.1074/jbc.R800035200.

[20]
C. R. Harwood and Y. Kikuchi, "The Ins and Outs of Bacillus Proteases: Activities, Functions and Commercial Significance," *FEMS Microbiol. Rev.*, vol. 46, no. 1, fuab046, 2022. [Online]. Available: https://doi.org/10.1093/femsre/fuab046.

[21]
Kirstein, J.; Hoffmann, A.; Lilie, H.; Schmidt, R.; Rübsamen-Waigmann, H.; Brötz-Oesterhelt, H.; Mogk, A.; Turgay, K. The AB ADEP reprogrammes ClpP, switching it from a regulated to an uncontrolled protease. *EMBO Molecular Medicine* 2009, *1*, 37–49. https://doi.org/10.1002/emmm.200900002

[22]
Imlay, J. A. The Molecular Mechanisms and Physiological Consequences of Oxidative Stress: Lessons from a Model Bacterium. *Nature Reviews Microbiology* 2013, 11, 443–454. https://doi.org/10.1038/nrmicro3032

[23]
Valle, A.; Oliver, J.; Roca, P. Role of Uncoupling Proteins in Cancer. *Cancers* 2010, 2, 567–591. https://doi.org/10.3390/cancers2020567

[24]
Borisov, V. B.; Siletsky, S. A.; Nastasi, M. R.; Forte, E. ROS Defense Systems and Terminal Oxidases in Bacteria. *Antioxidants* 2021, 10, 839. https://doi.org/10.3390/antiox10060839

[25]
Kohanski, M. A.; Dwyer, D. J.; Hayete, B.; Lawrence, C. A.; Collins, J. J. A Common Mechanism of Cellular Death Induced by Bactericidal Antibiotics. *Cell* 2007, 130, 797–810. https://doi.org/10.1016/j.cell.2007.06.049

[26]
Gaballa, A.; Su, T. T.; Helmann, J. D. *The Bacillus subtilis* monothiol bacilliredoxin BrxC (YtxJ) and the Bdr (YpdA) disulfide reductase reduce S-bacillithiolated proteins.* Redox Biology 2021, 42, 101935. https://doi.org/10.1016/j.redox.2021.101935

[27]
Van Acker, H.; Coenye, T. The Role of Reactive Oxygen Species in Antibiotic-Mediated Killing of Bacteria. *Trends in Microbiology* 2017, 25, 456–466. https://doi.org/10.1016/j.tim.2016.12.008

[28]
Schäfer, A.-B.; Wenzel, M. A How-To Guide for Mode of Action Analysis of Antimicrobial Peptides. *Frontiers in Cellular and Infection Microbiology* 2020, *10*. https://doi.org/10.3389/fcimb.2020.540898

[29]
Thermo Fisher Scientific. Reactive Oxygen Species—Table 18.1, *Molecular Probes Handbook*; accessed May 28 2025. https://www.thermofisher.com/us/en/home/references/molecular-probes-the-handbook/tables/reactive-oxygen-species.html

[30]
Taiwo, F. A. Mechanism of Tiron as Scavenger of Superoxide Ions and Free Electrons. *Spectroscopy* 2008, 22, 491–498. https://doi.org/10.3233/SPE-2008-0362

[31]
Chueca, B.; Pagán, R.; García-Gonzalo, D. Differential Mechanism of *Escherichia coli* Inactivation by (+)-Limonene as a Function of Cell Physiological State and Drug's Concentration. *PLoS ONE* 2014, 9, e94072. https://doi.org/10.1371/journal.pone.0094072

[32]
HORIBA Scientific. *What Is Fluorescence Spectroscopy?* HORIBA Fluorescence-Spectroscopy Technology Webpage, n.d.; accessed 30 May 2025. https://www.horiba.com/int/scientific/technologies/fluorescence-spectroscopy/what-is-fluorescence-spectroscopy/

[33]
Remington, S. J. Green Fluorescent Protein: A Perspective. *Protein Sci.* 2011, 20 (9), 1509 – 1519. https://doi.org/10.1002/pro.684

[34]
Tsien, R. Y. The Green Fluorescent Protein. *Annu. Rev. Biochem.* 1998, 67, 509 – 544. https://doi.org/10.1146/annurev.biochem.67.1.509

[35]
CactiStaccingCrane, "Stokes shift diagram," Wikimedia Commons, 7 Jan 2023. [Online]. Available: https://commons.wikimedia.org/wiki/File:Stokes_shift_diagram.svg.
CC BY 4.0. Accessed 15 Jun 2025.

[36]
D. Ilyin, “Jablonski Diagram of Fluorescence Only,” Wikimedia Commons, 7 Dec 2021. [Online]. Available: https://commons.wikimedia.org/wiki/File:Jablonski_Diagram_of_Fluorescence_Only-en.svg.
CC0 1.0 Public Domain Dedication. Accessed 15 Jun 2025.

[37]
P. Nonejuie, M. Burkart, K. Pogliano, and J. Pogliano, “Bacterial cytological profiling rapidly identifies the cellular pathways targeted by antibacterial molecules,” *Proc. Natl. Acad. Sci. USA*, vol. 110, pp. 16169–16174, 2013. https://doi.org/10.1073/pnas.1311066110

[38]
M. Wenzel *et al.*, “Antimicrobial-peptide modes of action resolved by bacterial cytological profiling,” *mBio*, vol. 9, e00802-18, 2018. https://doi.org/10.1128/mBio.00802-18

[39]
A.-B. Schäfer and M. Wenzel, “A how-to guide for mode-of-action analysis of antimicrobial peptides,” *Front. Cell. Infect. Microbiol.*, vol. 10, 540898, 2020. https://doi.org/10.3389/fcimb.2020.540898

[40]
Lenhart, J. S.; Brandes, E. R.; Schroeder, J. W.; Sorenson, R. J.; Showalter, H. D.; Simmons, L. A. RecO and RecR Are Necessary for RecA Loading in Response to DNA Damage and Replication Fork Stress. *Journal of Bacteriology* 2014, 196, 2851–2860. https://doi.org/10.1128/JB.01494-14

[41]
Anagnostopoulos, C.; Spizizen, J. Requirements for transformation in *Bacillus subtilis*. J. Bacteriol. 1961, 81, 741–746. https://doi.org/10.1128/jb.81.5.741-746.1961

[42]
D. Saeloh, V. Tipmanee, K. K. Jim, M. P. Dekker, W. Bitter, S. P. Voravuthikunchai, M. Wenzel, and L. W. Hamoen, “The novel antibiotic rhodomyrtone traps membrane proteins in vesicles with increased fluidity,” PLoS pathogens, vol. 14, no. 2, e1006876, 2018. DOI: 10.1371/journal.ppat.1006876

[43]
N. Jahn, S. Brantl, and H. Strahl, “Against the mainstream: The membrane-associated type i toxin bsrg from Bacillus subtilis interferes with cell envelope biosynthesis without increasing membrane permeability,” Molecular Microbiology, vol. 98, no. 4, pp. 651–666, 2015. DOI: 10.1111/mmi.13146.

[44]
CLSI. *Methods for Dilution Antimicrobial Susceptibility Tests for Bacteria That Grow Aerobically*, 12th ed.; CLSI Standard M07; Clinical and Laboratory Standards Institute: Wayne, PA, USA, 2024. ISBN 978-1-68440-226-7.

[45]
Te Winkel, J.D.; Gray, D.A.; Seistrup, K.H.; Hamoen, L.W.; Strahl, H. Analysis of Antimicrobial-Triggered Membrane Depolarization Using Voltage Sensitive Dyes. Front. Cell Dev. Biol. 2016, 4, 29. https://doi.org/10.3389/fcell.2016.00029

[46]
Schäfer A, Sidarta M, Abdelmesseh Nekhala I, Marinho Righetto G, Arshad A, Wenzel M. 2024. Dissecting AB effects on the cell envelope using bacterial cytological profiling: a phenotypic analysis starter kit. Microbiology Spectroscopy 12:e03275-23. https://doi.org/10.1128/spectrum.03275-23

[47]
Schäfer, A.-B.; Steenhuis, M.; Jim, K.K.; Neef, J.; O’Keefe, S.; Whitehead, R.C.; Swanton, E.; Wang, B.; Halbedel, S.; High, S.; van Dijl, J.M.; Luirink, J.; Wenzel, M. *Dual Action of Eeyarestatin 24 on Sec-Dependent*

*Protein Secretion and Bacterial DNA*. ACS Infect. Dis**.** 2023, 9, 253–269. https://doi.org/10.1021/acsinfecdis.2c00404

[48]
Schindelin, J.; Arganda-Carreras, I.; Frise, E.; et al. Fiji: An Open-Source Platform for Biological-Image Analysis. *Nature Methods* 2012, 9, 676–682. https://doi.org/10.1038/nmeth.2019

[49]
Syvertsson, S.; Vischer, N. O. E.; Gao, Y.; Hamoen, L. W. When Phase Contrast Fails: ChainTracer and NucTracer, Two ImageJ Methods for Semi-Automated Single Cell Analysis Using Membrane or DNA Staining. *PLoS ONE* 2016, 11, e0151267. https://doi.org/10.1371/journal.pone.0151267

[50]
Ducret, A.; Quardokus, E. M.; Brun, Y. V. MicrobeJ, a Tool for High-Throughput Bacterial Cell Detection and Quantitative Analysis. *Nature Microbiology* 2016, 1, 16077. https://doi.org/10.1038/nmicrobiol.2016.77

[51]
Strahl, H.; Bürmann, F.; Hamoen, L.W. *The actin homologue MreB organizes the bacterial cell membrane*. Nat. Commun. 2014, 5, 3442. https://doi.org/10.1038/ncomms4442

[52]
Wenzel, M.; Dekker, M.P.; Wang, B.; Burggraaf, M.J.; Bitter, W.; van Weering, J.R.T.; Hamoen, L.W. *A flat embedding method for transmission electron microscopy reveals an unknown mechanism of tetracycline*. Commun. Biol. 2021, 4, 306. https://doi.org/10.1038/s42003-021-01809-8

[53]
Halliwell, B.; Gutteridge, J. M. C. Biologically Relevant Metal Ion-Dependent Hydroxyl Radical Generation: An Update. *FEBS Letters* 1992, 307, 108–112. https://doi.org/10.1016/0014-5793(92)80911-Y

[54]
Kettler, P. B. Platinum Group Metals in Catalysis: Fabrication of Catalysts and Catalyst Precursors. *Organic Process Research & Development* 2003, 7, 342–354. https://doi.org/10.1021/op034017o

[55]
Weng, C.; Shen, L.; Teo, J. W.; Lim, Z. C.; Loh, B. S.; Ang, W. H. Targeted Antibacterial Strategy Based on Reactive Oxygen Species Generated from Dioxygen Reduction Using an Organoruthenium Complex. *JACS Au* 2021, 1, 1348–1354. https://doi.org/10.1021/jacsau.1c00262

## Appendix A - (Supplementary results)

### MIC

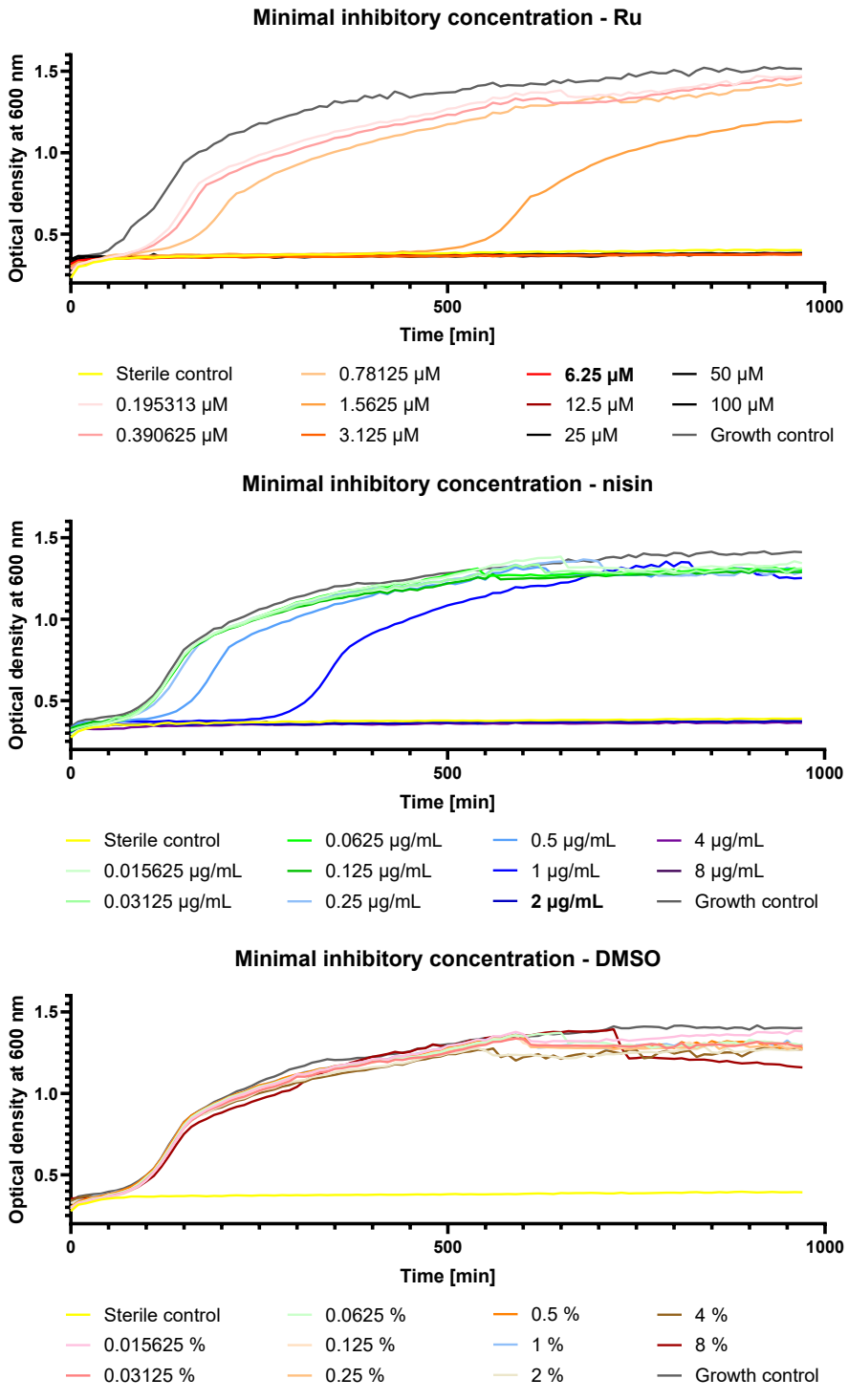


**16-hour growth curves for Ru (top), nisin (middle) and DMSO (bottom) treatments.** For each set (Ru, nisin, DMSO) the growth measured by optical density absorbance is plotted for 2-fold decreases of concentration. Sterile controls (yellow) for the three sets show no growth and the growth control (dark grey) show normal growth. Identified MIC values are marked in bold.

**BCP**

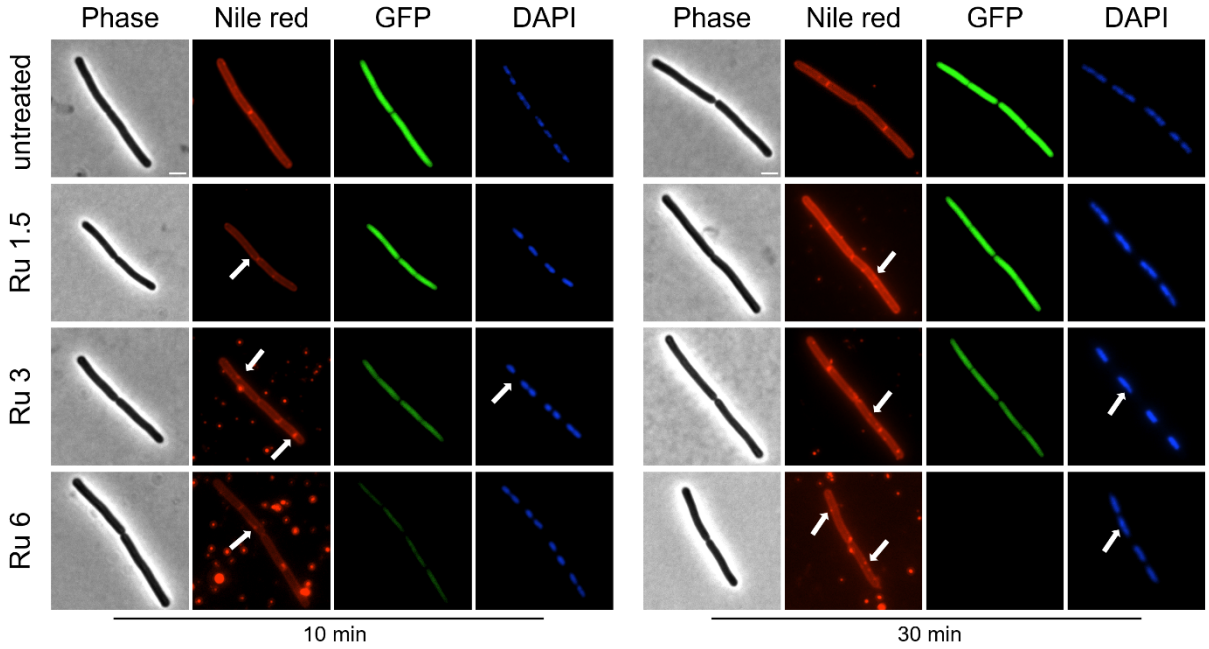


**Second replicate of BCP.** *B. subtilis* strain MW54 (*PrpsD-gfp*) treated for 10 and 30 minutes with Ru at concentrations of 1.5625 (1.5), 3.125 (3), and 6.25 µM (6), alongside an untreated sample. The GFP channel's brightness and contrast are scaled equally. Scale bar represents 2 µm. Arrows in Nile red point to membrane stress foci and in the DAPI at unevenly packed DNA.

**BCP-GFP**

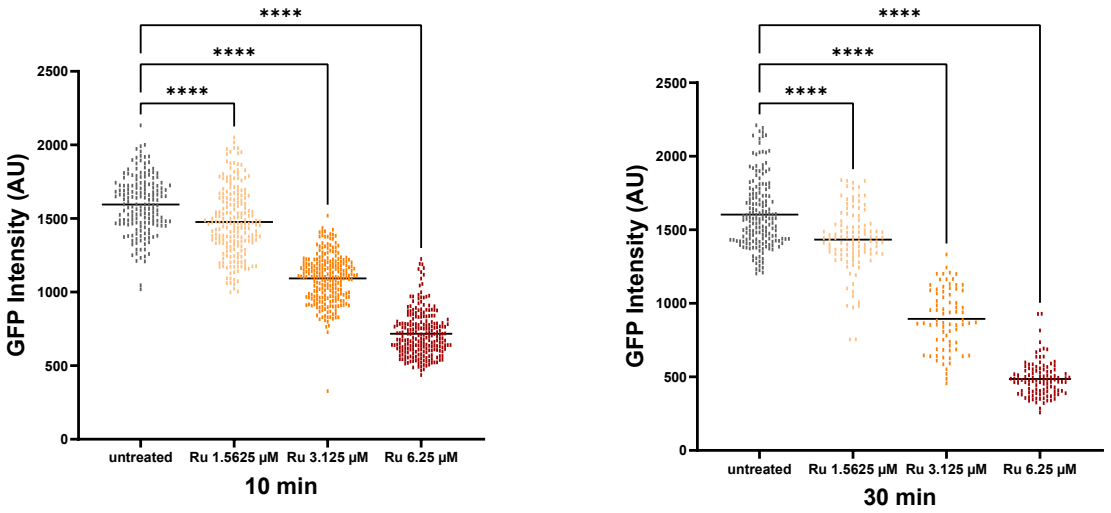


**First replicate of quantified GFP intensity in BCP after Ru treatment.** Scatter plots of GFP intensity data of *B. subtilis* MW54 (*PrpsD-gfp*) measured after 10 min (A) and 30 min (B) exposure to Ru (1.5625 µM, 3.125 µM, 6.25 µM) compared with an untreated control. Asterisks denote significance (****, $P < 0.0001$). Black horizontal bars indicate group means.

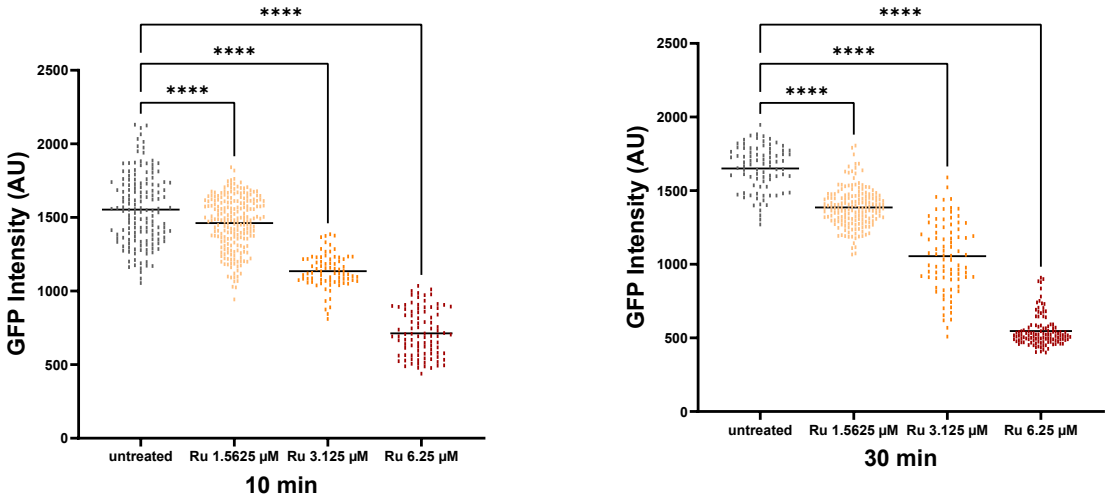


**Second replicate of quantified GFP intensity in BCP after Ru treatment.** Scatter plots of GFP intensity data of *B. subtilis* MW54 (*PrpsD-gfp*) measured after 10 min (A) and 30 min (B) exposure to Ru (1.5625 µM, 3.125 µM, 6.25 µM) compared with an untreated control. Asterisks denote significance (****, $P < 0.0001$). Black horizontal bars indicate group means.

**RecA-GFP**

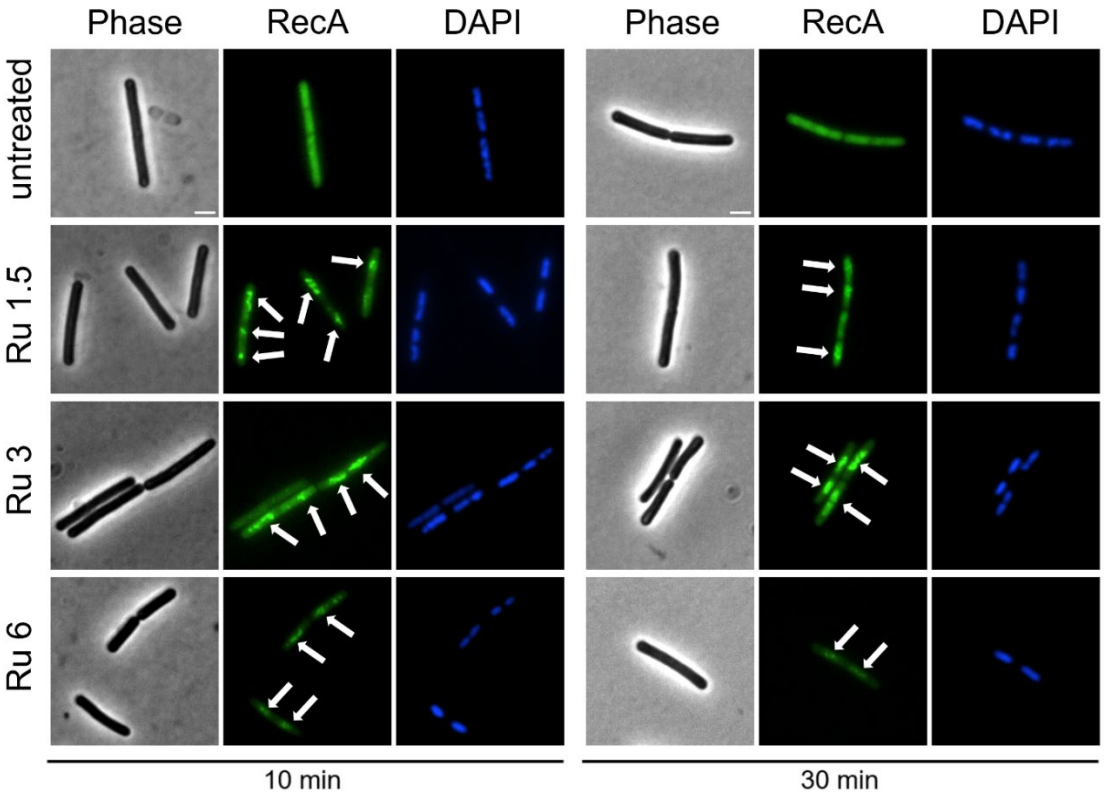


**Second replicate of RecA-GFP response to Ru-induced DNA damage.**
*B. subtilis* strain UG10 (*amyE::Pxyl-recA-mgfp* spc) treated for 10 and 30 minutes with Ru at concentrations of 1.5625 (1.5), 3.125 (3), and 6.25 µM (6), alongside an untreated sample. Untreated cells exhibit diffuse GFP, whereas Ru display discrete GFP foci marked with arrows. Arrows in DAPI point to DNA symmetry abnormalities. Scale bar represents 2 µm.

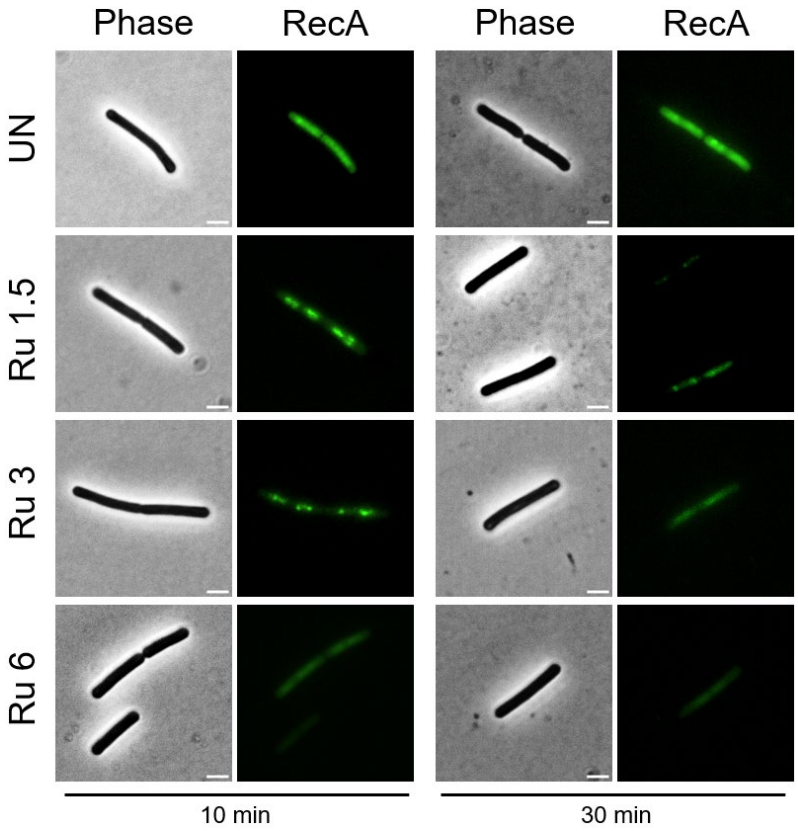


**Third replicate of RecA-GFP response to Ru-induced DNA damage.**
*B. subtilis* strain UG10 (*amyE::Pxyl-recA-mgfp* spc) treated for 10 and 30 minutes with Ru at concentrations of 1.5625 (1.5), 3.125 (3), and 6.25 µM (6), alongside an untreated sample. Untreated cells exhibit diffuse GFP, whereas Ru display discrete GFP foci. Scale bar represents 2 µm.

## Oxyburst

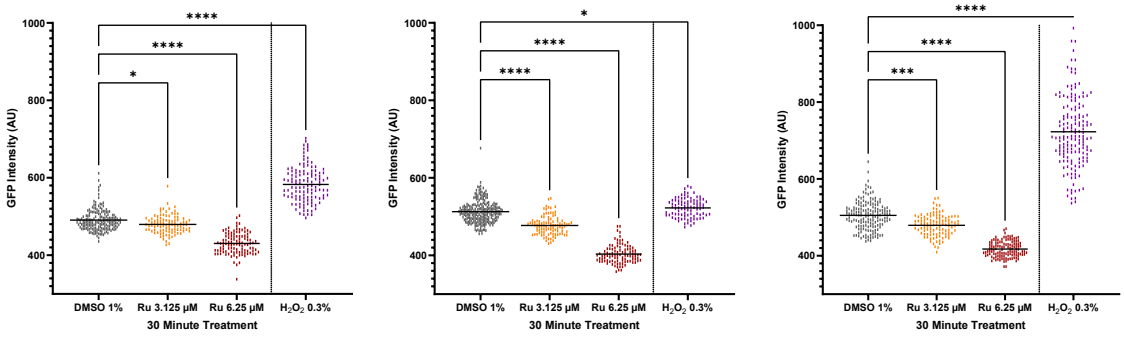


**Three replicates of intracellular superoxide presence after 30 min antibiotic treatment.** Scatter plots of Oxyburst fluorescence in *B. subtilis* for treatment with Ru (3.125 µM, 6.25 µM), 1% DMSO, and 0.3% $H_2O_2$. Asterisks indicate ANOVA significance. Black horizontal bars show the group mean intensities.

**GSS**

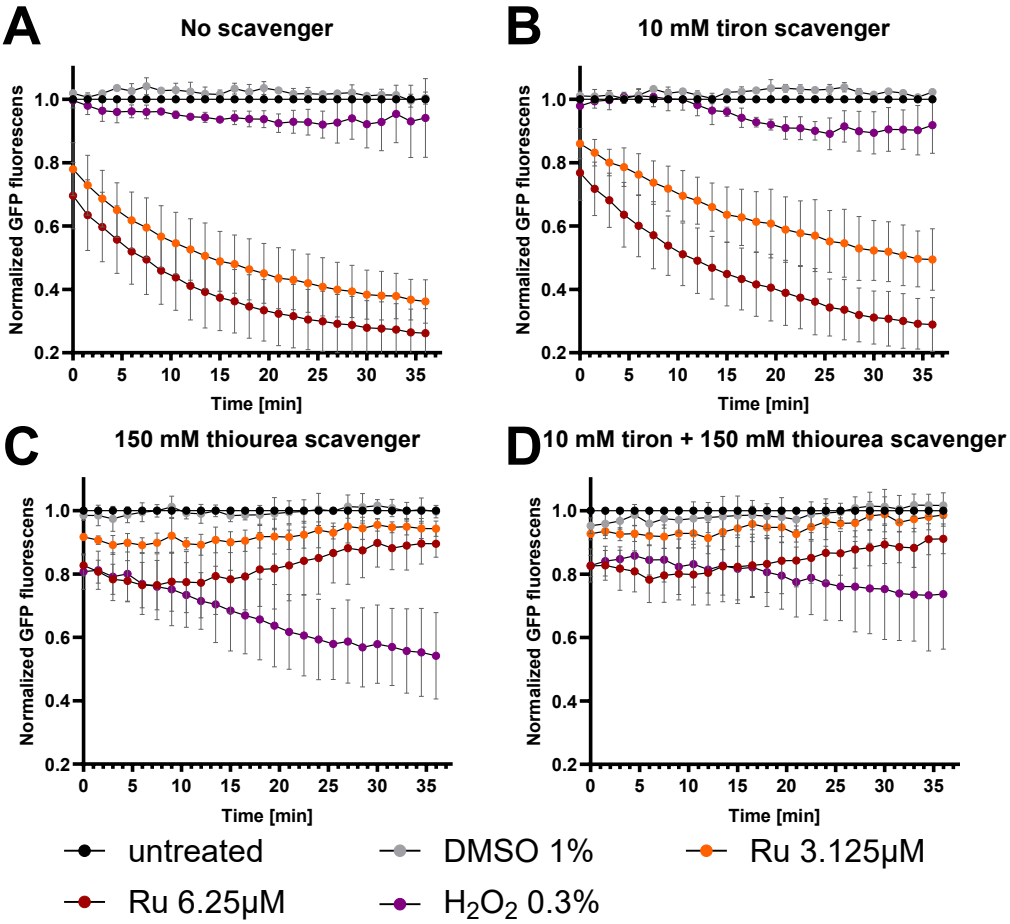


**GFP scavenger spectroscopy results.** Normalized GFP fluorescence intensity from three biological replicates (shown through error bars) of *B. subtilis* MW54 cultures. GFP signal was monitored every 90 seconds for 35 min after addition of cell cultures to a pre-prepared plate with antibiotics: no scavenger (A), 10 mM tiron (B) that targets $O_2^{\bullet -}$, 150 mM thiourea (C) that neutralizes OH• and the combined set with both thiourea and tiron (D).

## Appendix B - (Complementary methodology)

### OSC

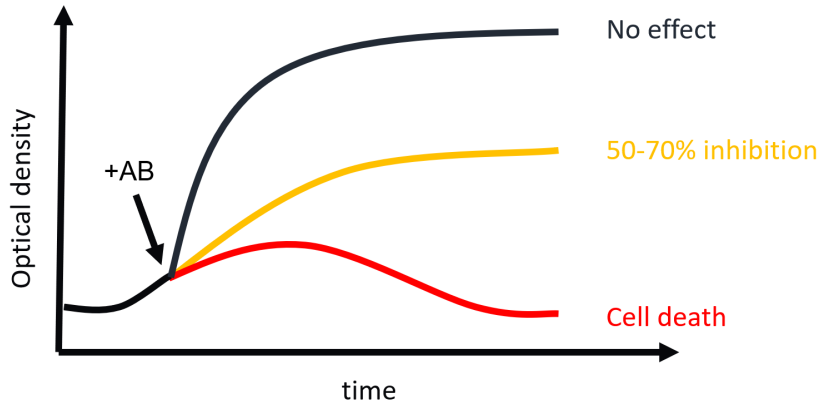


**Guide for picking the OSC.** Used here with permission of A. B. Schäfer.

### Image analysis

Using ObjectJ the BCP images were used to count individual cell membrane stress by identifying cells with foci not explained by septas. This was done according to the figure below:

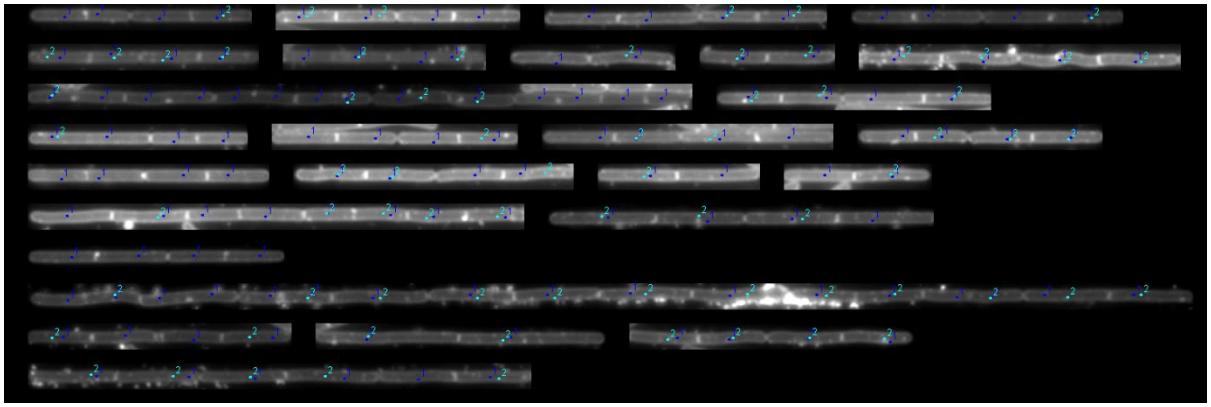

**Straightened out cell chains counted for membrane stress.** Identified chains from objectJ is first analyzed for individual cell count then using the NR channel and the counting tool in Fiji the cells who are stressed (turquoise markers) and all cells (deep blue markers) are counted

For the GFP and Oxyburst quantification the plugin MicrobeJ was used to first identify all the cell chain areas by phase contrast and area (>1 AU) filters. The chain selections were then cut into cells using NR and GFP information. The cells were then reviewed a last time before a final quantification of the mean signal for individual cells was made.

## Appendix C - (Instrument settings and metadata)

### MIC settings

| Parameter | Setting |
|---|---|
| Microplate | 96-well Falcon clear, flat-bottom; top read |
| Temperature | 38.5 °C constant (To achieve 37.0 °C) |
| Kinetic acquisition | 98 cycles; 600 s interval; 150 flashes per well per cycle |
| Scan mode | Spiral averaging; 6 mm diameter |
| Wavelength | 600 nm (single-wavelength absorbance) |
| Settling time | 0.5 s before each read |
| Scan pattern | Bidirectional, horizontal left-to-right, top-to-bottom |
| Atmospheric control | $O_2$ and $CO_2$ off (ambient conditions) |

### GSS settings

| Parameter | Setting |
|---|---|
| Microplate | 96-well Costar clear, flat-bottom; top read |
| Temperature | 38.5 °C constant (To achieve 37.0 °C) |
| Kinetic acquisition | 25 cycles; 90 s interval; 100 flashes per well per cycle |
| Optics (GFP preset) | Excitation 470 ± 7.5 nm |
| Gain | Enhanced dynamic range (auto-gain) |
| Focal height | 8.3 mm (auto-focus using well C2) |
| Settling time | 0.1 s before each read |
| Scan pattern | Bidirectional, horizontal left-to-right, top-to-bottom |
| Atmospheric control | $O_2$ and $CO_2$ off (ambient conditions) |

### Exposure settings

| | Assay | | |
|---|---|---|---|
| **Channel/Filter** | **BCP** | **RecA-GFP** | **Oxyburst** |
| Phase | 100ms, 15% | 100ms, 15% | 100ms, 15% |
| GFP | 100ms, 15% | 1s, 15% | 1s, 15% |
| mCherry | 200ms, 15% | -- | -- |
| DAPI | 100ms, 15% | 100ms, 15% | -- |

## Appendix D - (Javascript macros)

During the project during the image analysis there were certain operations identified as unnecessarily time consuming which prompted the use of ChatGPT to iteratively make two JavaScripts to save time. First, when presenting BCP microscopy it is common practice to convert file type and color spaces and make region of interest (ROI) selections before export. The first script, “BCP and RecA ImagePreparationPipeline_0.1.js” is designed to do these processes in the right order with a toggle for two channels (RecA) and 4 channels (BCP) with the options to tweak the ROI size, add tweakable scalebars with and without length written out. Once settings are all set, the individual channels export to respective .tif files with correct names.

The second script was made in preparation for image analysis using the ObjectJ and MicrobJ plugins in which especially the ObjectJ plugin requires certain file structures and new separate project files. The “BCP ObjJ channel rearrange_0.1” script automatically creates a new folder in the root folder of opened image files with the name of the image files and then pulls in a blank template project “.ojj” ObjectJ project file also renamed to the images names. This process often takes a lot of time with risk for user errors.

### BCP and RecA ImagePreparationPipeline_0.1.js :

```
importClass(Packages.ij.IJ);
importClass(Packages.ij.WindowManager);

importClass(Packages.javax.swing.JFrame);
importClass(Packages.javax.swing.JPanel);
importClass(Packages.javax.swing.JButton);
importClass(Packages.javax.swing.JCheckBox);
importClass(Packages.javax.swing.JComboBox);
importClass(Packages.javax.swing.JTextField);
importClass(Packages.javax.swing.JLabel);
importClass(Packages.javax.swing.BoxLayout);
importClass(Packages.javax.swing.BorderFactory);

importClass(Packages.java.awt.FlowLayout);
importClass(Packages.java.awt.Component);

/*********************************************************
 * Global data
 *********************************************************/

// ROI sizes that the user can pick (string array)
var roiSizeOptions = ["200","250","300","500"];

// We store references to UI fields so we can read their values
var roiSizeCombo    = null;   // for the ROI size
var assayCombo      = null;   // "BCP Assay" or "RecA Assay"
var scaleCheck      = null;   // checkbox "Add scale bar?"
var scaleCornerCombo= null;   // corner choice (Lower Right, etc.)
var scaleLengthField= null;   // text field for scale bar length
var scaleReadCheck  = null;   // checkbox for "Show length readout?"

// We'll store the currently chosen assay in a variable
var chosenAssay = "BCP Assay";

/*********************************************************
 * Script 1 (ROI Adjust):
 *  - Dynamically uses the chosen ROI size to resize
 *    the current selection, keeping x,y top-left unchanged.
 *********************************************************/
function buildScript1(roiSize) {
   // parse it or fallback
   var sizeVal = parseInt(roiSize, 10);
   if (isNaN(sizeVal)) sizeVal = 250;

   return ""
   + "getSelectionBounds(x, y, w, h);\n"
   + "makeRectangle(x, y, "+sizeVal+", "+sizeVal+");\n";
}

/*********************************************************
 * Script 2 (BCP Assay):
 * Phase => C4
 * DAPI => C1, GFP => C2, Nile => C3
 *********************************************************/
function buildScript2(scaleBarOn, barCorner, barLen, showLen) {
   var barCmd = "";
   if (scaleBarOn) {
      // build the scale bar command
      var cmd = "width="+barLen+" height=4 font=14 color=White background=None location=["+barCorner+"] hide overlay";
      if (showLen) {
```

```
            cmd += " show=length";
        }
        barCmd = "run(\"Scale Bar...\", \""+cmd+"\");\n";
    }

    return ""
    + "run(\"Crop\");\n"
    + "run(\"Split Channels\");\n"
    + "\n"
    // PHASE => C4
    + "list = getList(\"image.titles\");\n"
    + "for(i=0; i<list.length; i++){\n"
    + "  if(matches(list[i],\".*C4.*\")){\n"
    + "    selectWindow(list[i]);\n"
    + "  }\n"
    + "}\n"
    + barCmd
    + "run(\"Flatten\");\n"
    + "saveAs(\"Tiff\");\n"
    + "close();\n"
    + "\n"
    // C1 => DAPI
    + "list = getList(\"image.titles\");\n"
    + "for(i=0; i<list.length; i++){\n"
    + "  if(matches(list[i],\".*C1.*\")){\n"
    + "    selectWindow(list[i]);\n"
    + "  }\n"
    + "}\n"
    + "run(\"Copy\");\n"
    + "run(\"Flatten\");\n"
    + "saveAs(\"Tiff\");\n"
    + "close();\n"
    + "\n"
    // C2 => GFP
    + "list = getList(\"image.titles\");\n"
    + "for(i=0; i<list.length; i++){\n"
    + "  if(matches(list[i],\".*C2.*\")){\n"
    + "    selectWindow(list[i]);\n"
    + "  }\n"
    + "}\n"
    + "run(\"Copy\");\n"
    + "run(\"Flatten\");\n"
    + "saveAs(\"Tiff\");\n"
    + "close();\n"
    + "\n"
    // C3 => Nile
    + "list = getList(\"image.titles\");\n"
    + "for(i=0; i<list.length; i++){\n"
    + "  if(matches(list[i],\".*C3.*\")){\n"
    + "    selectWindow(list[i]);\n"
    + "  }\n"
    + "}\n"
    + "run(\"Copy\");\n"
    + "run(\"Flatten\");\n"
    + "saveAs(\"Tiff\");\n"
    + "close();\n";
}

/************************************************************
 * Script 3 (RecA Assay):
 * Phase => C2
 * GFP   => C1
 ************************************************************/
function buildScript3(scaleBarOn, barCorner, barLen, showLen) {
    var barCmd = "";
    if (scaleBarOn) {
        var cmd = "width="+barLen+" height=4 font=14 color=White background=None location=["+barCorner+"] hide overlay";
        if (showLen) {
            cmd += " show=length";
        }
        barCmd = "run(\"Scale Bar...\", \""+cmd+"\");\n";
    }

    return ""
    + "run(\"Crop\");\n"
    + "run(\"Split Channels\");\n"
    + "\n"
    // PHASE => C2
    + "list = getList(\"image.titles\");\n"
    + "for(i=0; i<list.length; i++){\n"
    + "  if(matches(list[i],\".*C2.*\")){\n"
    + "    selectWindow(list[i]);\n"
    + "  }\n"
    + "}\n"
    + barCmd
    + "run(\"Flatten\");\n"
    + "saveAs(\"Tiff\");\n"
    + "close();\n"
```

```
    + "\n"
    // GFP => C1
    + "list = getList(\"image.titles\");\n"
    + "for(i=0; i<list.length; i++){\n"
    + "  if(matches(list[i],\".*C1.*\")){\n"
    + "    selectWindow(list[i]);\n"
    + "  }\n"
    + "}\n"
    + "run(\"Copy\");\n"
    + "run(\"Flatten\");\n"
    + "saveAs(\"Tiff\");\n"
    + "close();\n";
}

/*****************************************************
 * buildMainWindow() - construct the UI
 *****************************************************/
function buildMainWindow() {
    var frame = new JFrame("Workflow Control");
    frame.setLayout(new BoxLayout(frame.getContentPane(), BoxLayout.Y_AXIS));
    frame.setSize(380, 600);

    // ========================
    // 1) "Adjustment" panel
    // ========================
    var adjPanel = new JPanel();
    adjPanel.setLayout(new BoxLayout(adjPanel, BoxLayout.Y_AXIS));
    adjPanel.setBorder(BorderFactory.createTitledBorder("Adjustment"));

    // -- B/C Window button
    var bcBtn = new JButton("Open B/C Window");
    bcBtn.addActionListener(function(e){
        IJ.run("Brightness/Contrast...");
    });
    adjPanel.add(bcBtn);

    // -- ROI row
    var roiRow = new JPanel(new FlowLayout());
    roiRow.add(new JLabel("ROI Size (µm):"));

    roiSizeCombo = new JComboBox(roiSizeOptions);
    roiSizeCombo.setSelectedItem("250");
    roiRow.add(roiSizeCombo);

    var roiAdjustBtn = new JButton("ROI Adjust");
    roiAdjustBtn.addActionListener(function(e){
        // read the selected ROI size
        var selectedSize = roiSizeCombo.getSelectedItem().toString();
        var macroStr = buildScript1(selectedSize);
        IJ.runMacro(macroStr);
    });
    roiRow.add(roiAdjustBtn);

    adjPanel.add(roiRow);
    frame.add(adjPanel);

    // ========================
    // 2) "Assay and Export Options"
    // ========================
    var assayPanel = new JPanel();
    assayPanel.setLayout(new BoxLayout(assayPanel, BoxLayout.Y_AXIS));
    assayPanel.setBorder(BorderFactory.createTitledBorder("Assay and Export Options"));

    // -- Assay row
    var assayRow = new JPanel(new FlowLayout());
    assayRow.add(new JLabel("Select Assay:"));

    assayCombo = new JComboBox(["BCP Assay","RecA Assay"]);
    assayCombo.setSelectedItem("BCP Assay");
    assayCombo.addActionListener(function(e){
        chosenAssay = assayCombo.getSelectedItem().toString();
    });
    assayRow.add(assayCombo);

    assayPanel.add(assayRow);

    // -- Scale bar checkbox
    scaleCheck = new JCheckBox("Add scale bar on phase channel?", false);
    assayPanel.add(scaleCheck);

    // -- Scale bar position
    var barPosRow = new JPanel(new FlowLayout());
    barPosRow.add(new JLabel("Scale Bar Position:"));
    scaleCornerCombo = new JComboBox(["Lower Right","Lower Left","Upper Right","Upper Left"]);
    scaleCornerCombo.setSelectedItem("Lower Right");
    barPosRow.add(scaleCornerCombo);
    assayPanel.add(barPosRow);
```

```
    // -- Scale bar length
    var barLenRow = new JPanel(new FlowLayout());
    barLenRow.add(new JLabel("Scale Bar Length (µm):"));
    scaleLengthField = new JTextField("2", 5);
    barLenRow.add(scaleLengthField);
    assayPanel.add(barLenRow);

    // -- Show length readout?
    scaleReadCheck = new JCheckBox("Show length readout?");
    assayPanel.add(scaleReadCheck);

    // ========== A sub-panel for the "Export" button
    var exportPanel = new JPanel(new FlowLayout());
    exportPanel.setBorder(BorderFactory.createTitledBorder("Export"));

    var exportBtn = new JButton("Export");
    exportBtn.addActionListener(function(e){
       // read the latest UI settings
       var sbApply = scaleCheck.isSelected();
       var sbCorner= scaleCornerCombo.getSelectedItem().toString();
       var sbLen   = scaleLengthField.getText();
       var sbRead  = scaleReadCheck.isSelected();

       if (chosenAssay=="BCP Assay") {
          var macro = buildScript2(sbApply, sbCorner, sbLen, sbRead);
          IJ.runMacro(macro);
       } else {
          var macro2= buildScript3(sbApply, sbCorner, sbLen, sbRead);
          IJ.runMacro(macro2);
       }
    });
    exportPanel.add(exportBtn);

    assayPanel.add(exportPanel);

    frame.add(assayPanel);

    // ========================
    // 3) File Operations panel
    // ========================
    var filePanel = new JPanel();
    filePanel.setLayout(new BoxLayout(filePanel, BoxLayout.Y_AXIS));
    filePanel.setBorder(BorderFactory.createTitledBorder("File Operations"));

    // -- Open Another File
    var openFileBtn = new JButton("Open Another File");
    openFileBtn.addActionListener(function(e){
       closeAllImages();
       openFile();
    });
    filePanel.add(openFileBtn);

    // -- Close All Windows
    var closeAllBtn = new JButton("Close All Windows");
    closeAllBtn.addActionListener(function(e){
       closeAllImages();
    });
    filePanel.add(closeAllBtn);

    frame.add(filePanel);

    // ========================
    // 4) Footer text (left-aligned)
    // ========================
    var footerPanel = new JPanel();
    footerPanel.setLayout(new BoxLayout(footerPanel, BoxLayout.Y_AXIS));
    footerPanel.setAlignmentX(Component.LEFT_ALIGNMENT);

    // Use FlowLayout(FlowLayout.LEFT) to ensure left alignment
    // or we can do BoxLayout. We'll do BoxLayout and set each label's alignment
    var label1 = new JLabel("Wenzel Lab");
    label1.setAlignmentX(Component.LEFT_ALIGNMENT);
    var label2 = new JLabel("Made by Ann-Britt Schäfer");
    label2.setAlignmentX(Component.LEFT_ALIGNMENT);
    var label3 = new JLabel("Compiled by Robin Rydbergh (Using ChatGPT o1)");
    label3.setAlignmentX(Component.LEFT_ALIGNMENT);
    var label4 = new JLabel("2025/02/21");
    label4.setAlignmentX(Component.LEFT_ALIGNMENT);

    footerPanel.add(label1);
    footerPanel.add(label2);
    footerPanel.add(label3);
    footerPanel.add(label4);

    frame.add(footerPanel);

    frame.setVisible(true);
}
```

```
/*****************************************************
 * openFile() => pick a file, open it
 *****************************************************/
function openFile() {
    var path = IJ.getFilePath("Select an image file");
    if (!path) {
        IJ.log("No file selected.");
        return;
    }
    IJ.open(path);
    IJ.log("Opened => " + path);
}

/*****************************************************
 * closeAllImages() => closes any open images
 *****************************************************/
function closeAllImages() {
    var titles = WindowManager.getImageTitles();
    for (var i=0; i<titles.length; i++){
        var img = WindowManager.getImage(titles[i]);
        if (img) img.close();
    }
    IJ.log("Closed all images.");
}

// Build the UI
buildMainWindow();
```

# BCP ObjJ channel rearrange_0.1:

```
importClass(Packages.ij.IJ);
importClass(Packages.ij.WindowManager);
importClass(Packages.ij.io.FileInfo);
importClass(Packages.java.io.File);
importClass(Packages.java.nio.file.Files);
importClass(Packages.java.nio.file.Paths);
importClass(Packages.java.nio.file.StandardCopyOption);
importClass(Packages.javax.swing.JFrame);
importClass(Packages.javax.swing.JPanel);
importClass(Packages.javax.swing.JButton);
importClass(Packages.javax.swing.JCheckBox);
importClass(Packages.javax.swing.JComboBox);
importClass(Packages.javax.swing.JTextField);
importClass(Packages.javax.swing.JLabel);
importClass(Packages.javax.swing.BoxLayout);
importClass(Packages.javax.swing.BorderFactory);
importClass(Packages.java.awt.FlowLayout);
importClass(Packages.java.awt.Component);

/**
 * Main function to build a non-modal UI with three panels:
 *  1) "Open and adjust" instructions
 *  2) "Run" panel with a button that triggers rearrangeAndCopyOJJ()
 *  3) "Info" panel
 */
function buildUserInterface() {
    var frame = new JFrame("BCP Channel rearrange");
    frame.setLayout(new BoxLayout(frame.getContentPane(), BoxLayout.Y_AXIS));
    frame.setSize(380, 200);

    // ===== 1) OPEN AND ADJUST PANEL =====
    var openAdjustPanel = new JPanel();
    openAdjustPanel.setLayout(new BoxLayout(openAdjustPanel, BoxLayout.Y_AXIS));
    openAdjustPanel.setBorder(BorderFactory.createTitledBorder("Open and adjust the images to be rearranged"));

    // Just a label telling user to open images (via Fiji) and adjust them.
    var labelOpen = new JLabel("Use Fiji's File > Open or drag them in, then adjust as needed.");
    labelOpen.setAlignmentX(Component.LEFT_ALIGNMENT);
    openAdjustPanel.add(labelOpen);

    // Add the panel to the main frame
    frame.add(openAdjustPanel);

    // ===== 2) RUN PANEL =====
    var runPanel = new JPanel();
    runPanel.setLayout(new BoxLayout(runPanel, BoxLayout.Y_AXIS));
    runPanel.setBorder(BorderFactory.createTitledBorder("Run"));

    // A button that triggers the rearrange code
    var runBtn = new JButton("Run");
    runBtn.addActionListener(function(e){
        rearrangeAndCopyOJJ();
    });
    runPanel.add(runBtn);

    frame.add(runPanel);

    // ===== 3) INFO PANEL =====
    var infoPanel = new JPanel();
    infoPanel.setLayout(new BoxLayout(infoPanel, BoxLayout.Y_AXIS));
    infoPanel.setAlignmentX(Component.LEFT_ALIGNMENT);

    var label1 = new JLabel("Wenzel Lab");
    label1.setAlignmentX(Component.LEFT_ALIGNMENT);
    var label2 = new JLabel("Made by Robin Rydbergh (ChatGPT o1)");
    label2.setAlignmentX(Component.LEFT_ALIGNMENT);
    var label3 = new JLabel("Based on initial script by Gabriela Marinho Righetto");
    label3.setAlignmentX(Component.LEFT_ALIGNMENT);
    var label4 = new JLabel("2025/03/05");
    label4.setAlignmentX(Component.LEFT_ALIGNMENT);

    infoPanel.add(label1);
    infoPanel.add(label2);
    infoPanel.add(label3);
    infoPanel.add(label4);

    frame.add(infoPanel);

    frame.setVisible(true);
}

/**
 * Function that handles rearranging all open images in reverse order,
 * saving them in a newly created folder (based on the first image's filename),
 * and copying "Coli-Inspector-04g.ojj" from Fiji's scripts folder, renamed
 * to match the new folder name.
 */
function rearrangeAndCopyOJJ() {
    var titles = WindowManager.getImageTitles();
    if (titles.length === 0) {
        IJ.log("No images are open. Please open some first.");
        return;
    }

    var folderCreated = false;
```

```
    var saveFolder = null;
    var baseName = null;

    // Loop backward so closing each won't shift the rest
    for (var i = titles.length - 1; i >= 0; i--) {
        IJ.selectWindow(titles[i]);
        IJ.wait(200);

        var imp = WindowManager.getImage(titles[i]);
        if (!imp) {
            IJ.log("Could not retrieve ImagePlus for: " + titles[i]);
            continue;
        }

        // Original file info
        var fi = imp.getOriginalFileInfo();
        var directory = null;
        var filename  = null;
        if (fi != null) {
            directory = fi.directory;
            filename  = fi.fileName;
        } else {
            directory = IJ.getDirectory("Pick a folder to save " + titles[i]);
            if (directory == null) {
                IJ.log("User canceled saving " + titles[i]);
                imp.close();
                continue;
            }
            filename = titles[i] + ".tif";
        }

        // Create new folder if not done yet, based on first image's name
        if (!folderCreated) {
            baseName = filename;
            // Suppose we remove last 8 chars (e.g. .tif / .nd2).
            // Adjust if your naming pattern is different
            if (baseName.length > 8) {
                baseName = baseName.substring(0, baseName.length - 8);
            }
            saveFolder = directory + baseName;

            var newDir = new File(saveFolder);
            if (!newDir.exists()) {
                newDir.mkdirs();
                IJ.log("Created new folder => " + saveFolder);
            } else {
                IJ.log("Folder already exists => " + saveFolder);
            }
            folderCreated = true;
        }

        // 1) Rearrange channels
        IJ.run("Arrange Channels...", "new=4321");
        IJ.wait(200);

        // 2) Save
        var outPath = saveFolder + File.separator + filename;
        IJ.saveAs("Tiff", outPath);
        IJ.log("Rearranged & saved => " + outPath);

        // 3) Close image
        imp.close();
    }

    // If we created the new folder, copy "Coli-Inspector-04g.ojj" into it, renamed to baseName.ojj
    if (folderCreated && saveFolder != null && baseName != null) {
        var fijiDir = IJ.getDirectory("imagej");
        if (fijiDir == null) {
            IJ.log("Cannot detect Fiji installation directory. Cannot copy Coli-Inspector-04g.ojj");
        } else {
            var sourcePath = fijiDir + "scripts" + File.separator + "Coli-Inspector-04g.ojj";
            var sourceFile = new File(sourcePath);
            if (!sourceFile.exists()) {
                IJ.log("ERROR: 'Coli-Inspector-04g.ojj' not found in Fiji's scripts folder.\nPlease place it there!");
            } else {
                var destPath = saveFolder + File.separator + baseName + ".ojj";
                var destFile = new File(destPath);

                try {
                    Files.copy(
                        sourceFile.toPath(),
                        destFile.toPath(),
                        java.nio.file.StandardCopyOption.REPLACE_EXISTING
                    );
                    IJ.log("Copied OJJ => " + destPath);
                } catch(e) {
                    IJ.log("ERROR copying OJJ: " + e);
                }
            }
        }
    }

    // Close the images (already done individually),
    // but let's ensure we don't leave anything.
    IJ.run("Close All");
    IJ.log("All images rearranged & saved; OJJ copied (if found).");
}

// Build the UI immediately
buildUserInterface();
```

DEPARTMENT OF LIFE SCIENCES
CHALMERS UNIVERSITY OF TECHNOLOGY
Gothenburg, Sweden 2025
www.chalmers.se


CHALMERS
UNIVERSITY OF TECHNOLOGY